Pyruvate-GPR31 axis induces LysoDC dendrite protrusion to M-cell pockets for effective immune responses

Nakanishi, Katsuhiro
Laboratory of Microbiology and Immunology, School of Pharmaceutical Sciences, University of Shizuoka

Ajiro, Takayuki
Laboratory of Microbiology and Immunology, School of Pharmaceutical Sciences, University of Shizuoka

Yukishima, Kaito
Laboratory of Microbiology and Immunology, School of Pharmaceutical Sciences, University of Shizuoka
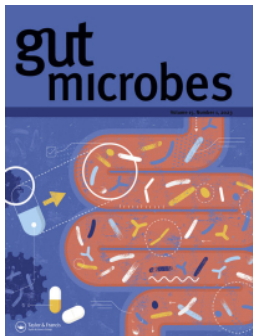
Tsukamoto, Yuki
Laboratory of Microbiology and Immunology, School of Pharmaceutical Sciences, University of Shizuoka

他

Pyruvate–GPR31 axis induces LysoDC dendrite protrusion to M-cell pockets for effective immune responses

Katsuhiro Nakanishi , Takayuki Ajiro , Kaito Yukishima , Yuki Tsukamoto , Junichi Kikuta , Shinichiro Sawa , Michio Tomura , Nozomi Kinoshita , Wataru Shimanuki , Akio Suzuki , Shun Arai , Kazuki Maeshima , Takumi Ichisawa , Tomoya Katakai , Haruko Hayasaka , Masaru Ishii & Eiji Umemoto

RESEARCH PAPER

Pyruvate–GPR31 axis induces LysoDC dendrite protrusion to M-cell pockets for effective immune responses

Katsuhiro Nakanishi[a]*, Takayuki Ajiro[a]*, Kaito Yukishima[a], Yuki Tsukamoto[a], Junichi Kikuta[b,c,d], Shinichiro Sawa[e], Michio Tomura[f], Nozomi Kinoshita[a], Wataru Shimanuki[a], Akio Suzuki[b], Shun Arai[a], Kazuki Maeshima[a], Takumi Ichisawa[a], Tomoya Katakai[g], Haruko Hayasaka[h], Masaru Ishii[c,d,i,j], and Eiji Umemoto [ID][a]

[a]Laboratory of Microbiology and Immunology, School of Pharmaceutical Sciences, University of Shizuoka, Shizuoka, Japan; [b]Division of Immunology, Department of Future Medical Sciences, Graduate School of Medicine, Kobe University, Hyogo, Japan; [c]Department of Immunology and Cell Biology, Graduate School of Medicine, Osaka University, Osaka, Japan; [d]Laboratory of Bioimaging and Drug Discovery, National Institutes of Biomedical Innovation, Health and Nutrition, Osaka, Japan; [e]Division of Mucosal Immunology, Research Center for Systems Immunology, Medical Institute of Bioregulation, Kyushu University, Fukuoka, Japan; [f]Laboratory of Immunology, Faculty of Pharmacy, Osaka Ohtani University, Osaka, Japan; [g]Department of Immunology, Niigata University Graduate School of Medical and Dental Sciences, Niigata, Japan; [h]Department of Life Science, Faculty of Science & Engineering, Kindai University, Osaka, Japan; [i]Department of Immunology and Cell Biology, WPI-Immunology Frontier Research Center, Osaka University, Osaka, Japan; [j]Life-omics Research Division, Institute for Open and Transdisciplinary Research Initiative, Osaka University, Osaka, Japan

ABSTRACT

Peyer's patches (PPs) are sites of antigen entry and immunoinduction in the small intestine. In PPs, pathogens are transferred through microfold (M) cells; however, the mechanisms of antigen capture by mononuclear phagocytes beneath M cells remain unclear. Here, we demonstrate that bacterial metabolite pyruvate acted on lysozyme-expressing dendritic cells (LysoDCs), a monocyte-derived phagocyte subset, and induced protrusion of dendrites particularly with "balloon" shapes into basolateral M-cell pockets via its receptor, G-protein coupled receptor 31 (GPR31). Pyruvate administration in wild-type but not Gpr31b-deficient mice increased LysoDC uptake of orally infected Listeria monocytogenes. GPR31 signaling boosted antigen processing and altered gene expression. It also increased LysoDC migration to the interfollicular region, thereby promoting production of pathogen-specific Th1 cells as well as cytotoxic T cells, and effector T cell migration to the lamina propria. Furthermore, oral pyruvate administration conferred high resistance to a virulent L. monocytogenes strain in a GPR31-dependent manner. Collectively, the pyruvate – GPR31 axis plays critical roles in orchestrating intestinal protective immunity.

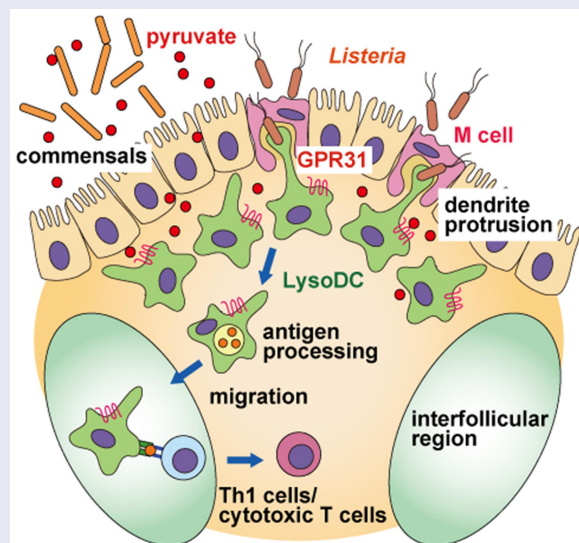**CONTACT** Eiji Umemoto eumemoto@u-shizuoka-ken.ac.jp Laboratory of Microbiology and Immunology, School of Pharmaceutical Sciences, University of Shizuoka, 52-1 Yada, Suruga, Shizuoka 422-8526, Japan
*These authors contributed equally to this work.

Introduction

Peyer's patches (PPs) are lymphoid tissues of the small intestine that serve as entry sites for intestinal pathogens and initiate adaptive immune responses.[1] They contain several clustered B-cell follicles interspersed with T-cell zones, which are termed interfollicular regions (IFRs). The follicle-associated epithelium (FAE) is equipped with speciaportlized epithelial cells – microfold (M) cells – that efficiently transcytose exogenous luminal antigens and deliver them to the underlying subepithelial dome (SED), a region enriched in mononuclear phagocytes (MNPs).[2,3]

M cells mediate the uptake of a variety of pathogenic microorganisms. They express a glycosylphosphatidylinositol-anchored protein, glycoprotein 2 (GP2), that acts as a receptor for FimH, a component of type I pili-expressing bacteria such as *Salmonella enterica* serovar Typhimurium (hereafter *S.* Typhimurium) and *Escherichia coli* .[4] They also serve as a portal of initial invasion for other enteropathogenic bacteria, including *Brucella abortus, Shigella flexneri*, and *Yersinia enterocolitica*.[5-8] In humans, *Listeria monocytogenes* mainly invades the lamina propria (LP) of the small intestine through interactions between its surface protein internalin A (InlA) and luminally accessible E-cadherin on epithelial cells (including goblet cells)[9]; however, InlA does not bind to murine E-cadherin because it differs by a single amino acid that is responsible for its interaction with inlA.[10,11] In mice, *L. monocytogenes* is preferentially transferred through M cells[8] in an InlA-independent manner.[12,13] Morphologically, M cells lack the typical brush border found in intestinal epithelial cells and their apical surfaces have broad membrane microdomains that are suitable for endocytosis. The M-cell basolateral membrane is deeply invaginated to form basolateral pockets, which provide a specialized microenvironment beneath the FAE. The M-cell pocket enables phagocytes to easily access transcytosed pathogens and rapidly initiate immune responses.[14,15]

CD11c$^+$ myeloid cells in PPs are classified into five populations: conventional type 1 dendritic cells (cDC1s); conventional type 2 DCs (cDC2s), which include CD11b$^+$ and CD11b$^-$ subpopulations; plasmacytoid DCs; lysozyme-expressing DCs (LysoDCs); and lysozyme-expressing macrophages (LysoMacs), which can be further divided into Tim-4$^+$ and Tim-4$^-$ populations.[16,17] LysoDCs and LysoMacs are derived from monocytes and phenotypically share CX3CR1 and MerTK expression. These cells can be distinguished by their expression levels of MHC class II, CD4, and CD11b (LysoDCs: MHC class II^{high} CD4$^-$ CD11b^{high}; LysoMacs: MHC class II^{low} CD4$^+$ CD11b^{intermediate}). cDC1s and plasmacytoid DCs are concentrated in the IFR, whereas cDC2s reside in both the SED and IFR. Mature LysoDCs show preferential localization in the SED and closely interact with M cells.[18] They extend dendritic processes along M-cell pockets[19] and efficiently take up particulate antigens[20] as well as pathogenic bacteria such as *S.* Typhimurium.[21] They also recognize pathogens through the expression of Toll-like receptors (TLRs) and C-type lectin Mincle for the production of tumor necrosis factor-α, interleukin (IL)-6, and IL-23.[20,22] Although LysoDCs do not migrate into the IFR under steady-state conditions, they express CCR7 upon stimulation and migrate from the SED to the IFR periphery.[18] They then prime naïve CD4$^+$ T cells for interferon (IFN)-γ and IL-17 production,[20,22] and the LysoDC population that expresses complement receptor C5aR mediates cross-presentation to induce antigen-specific CD8$^+$ T cells.[23] Thus, a close association between LysoDCs in the SED and M cells enhances phagocytosis and plays an important role in both innate defense and adaptive immune induction.

The preferential distribution of DCs in the SED is regulated by chemokines and chemokine receptors. The FAE constitutively produces multiple chemokines including CCL20, CCL9, and CXCL16.[14,24,25] Upon *S.* Typhimurium infection, DCs that express CCR6 (a CCL20 receptor) are rapidly recruited to the FAE and induce T cell activation in a CCR6-dependent manner.[26] CCR6$^+$ DCs are distinct from CX3CR1$^+$ cells (LysoDCs and LysoMacs), which lack CCR6 expression.[26] CCL9 expression is dependent on transcription factor Spi-B, which regulates M-cell differentiation.[27] Functional blockage of CCL9 results in reduced CD11b$^+$ DCs (presumably including LysoDCs) in the SED under steady-state conditions, whereas CCR6 deficiency does not.[28] Although these data indicate that FAE-derived chemokines contribute to DC migration to the SED, the molecular mechanisms by which LysoDCs residing just beneath the FAE extend their dendrites to M cells, and the significance of dendrite protrusion by LysoDCs on the induction of adaptive immune responses, remain unclear.

In the LP of the small intestine, CX3CR1$^+$ MNPs extend their dendrites between adjacent epithelial cells and into the lumen for bacteria uptake.[29] Although they originate from circulating monocytes, their differentiation is largely dependent on macrophage colony-stimulating factor receptor.[30] Unlike LysoDCs, these MNPs are not very motile and transfer antigens to CD103$^+$ DCs via gap junctions.[31] We have previously reported that transepithelial dendrite protrusion by CX3CR1$^+$ MNPs is mediated by commensal bacterial metabolites – pyruvate and L-/D-lactate – and their receptor, G-protein coupled receptor 31 (GPR31).[32] GPR31 is preferentially expressed by CX3CR1$^+$ MNPs in the small intestine.[32] Although GPR31 signaling enhances oral tolerance to food antigens under steady-state conditions,[33] oral pyruvate or lactate administration promotes immune responses and a high resistance to intestinal *S.* Typhimurium infection in a GPR31-dependent manner.[32]

In the present study, we investigated the role of the pyruvate – GPR31 axis in dendrite protrusion of LysoDCs and induction of adaptive immune responses in PPs using a mouse model of *L. monocytogenes* infection. The pyruvate/GPR31-dependent dendrite protrusion from LysoDCs to basolateral M-cell pockets provides molecular insights into protective intestinal immunity against pathogenic bacteria.

Materials and methods

Mice

Six- to twenty-week-old C57BL6/J mice (male or female) were purchased from Japan SLC. Three to five mice were housed per cage with free access to food and water under a strict 12-h light cycle. The *Gpr31b*$^{-/-}$ mice, *Cx3cr1*$^{gfp/gfp}$ mice, and KikGR knock-in mice were described previously.[32,34,35] The mice were maintained under specific pathogen-free conditions. All animal experiments were conducted following the guidelines of University of Shizuoka, using procedures approved by the Animal Care and Use Committee of the University of Shizuoka.

L. monocytogenes

The *L. monocytogenes* strain EGDe was purchased from American Type Culture Collection (BAA-679). The *L. monocytogenes* strain 10403S was kindly provided by Dr. Hitomi Mimuro (Oita University). Bacteria were cultured in brain heart infusion medium (BD Biosciences). For oral administration, *L. monocytogenes* was suspended in 5% sodium bicarbonate.

Cell preparation

For the preparation of PP cells, PP tissue was cut into small pieces and digested in digestion solution (RPMI 1640 containing 5% fetal calf serum, 400 Mandl U/mL of collagenase D [Roche], and 100 μg/mL of DNase I [Sigma-Aldrich]) with continuous stirring at 37°C for 40 min. Cells in the small intestine were prepared as described previously.[36] Briefly, small intestinal tissue was opened longitudinally and washed extensively with PBS after PPs were removed. Small intestinal segments were incubated at 37°C for 30 min in PBS containing 10 mM ethylenediaminetetraacetic acid and 2% fetal calf serum before being washed several times with PBS. The small intestinal segments were then digested in digestion solution with continuous stirring at 37°C for 50 min. Lymphocytes in the small intestine were enriched by density gradient centrifugation using 40% and 80% Percoll (GE Healthcare).

Flow cytometry

The prepared cells were pretreated with anti-CD16/32 monoclonal antibody (mAb) to block nonspecific binding before being incubated with anti-cell-surface marker mAbs. For cytokine staining, cells were fixed and permeabilized with BD Fixation/Permeabilization solution (BD Biosciences) and intracellularly stained with anti-cytokine mAbs. To detect chemokine binding, PPs were collected 2 days after infection. Cells were incubated with soluble chemokine chimeras containing the human IgG$_1$ constant region (CCL19-Fc,

CXCL12-Fc, and Human IgG-Fc; gifts from Dr. Hieshima, Kindai University),[37] followed by anti-human IgG (H+L) F(ab')$_2$ fragment. Cells from *L. monocytogenes*-infected mice were fixed in phosphate buffer containing 4% paraformaldehyde to inactivate *L. monocytogenes*. Flow cytometric analysis was then performed using CytoFLEX (Beckman Coulter) with FlowJo software (version 10; BD Biosciences). Antibodies are listed in Table S1. Cell populations were gated as follows: LysoDCs (CX3CR1^{high} CD11c^{high} CD4$^-$ MHC class II^{high} or MerTK$^+$ CD11c^{high} CD4$^-$ MHC class II^{high}), Tim-4$^-$ LysoMacs (CX3CR1^{high} CD11c^{high} CD4$^+$ MHC class II^{low} Tim-4$^-$), and Tim-4$^+$ LysoMacs (CX3CR1^{high} CD11c^{high} CD4$^+$ MHC class II^{low} Tim-4$^+$), cDCs (MerTK$^-$ CD11c^{high} MHC class II^{high}), Th1 cells (T cell receptor beta [TCRβ$^+$ CD4$^+$ IFN-γ$^+$ IL-17$^-$], Th17 cells (TCRβ$^+$ CD4$^+$ IFN-γ$^-$ IL-17$^+$), effector CD4$^+$ T cells (TCRβ$^+$ CD4$^+$ CD62L$^-$ CD44$^+$), and effector CD8$^+$ T cells (TCRβ$^+$ CD8$^+$ CD62L$^-$ CD44$^+$).

RNA extraction and quantitative PCR

PP cells were prepared from *Gpr31b$^{+/+}$ Cx3cr1$^{gfp/+}$* mice as described in the *Cell preparation* section. The cells were pretreated with anti-CD16/32 mAb to block nonspecific binding before being incubated with PE-anti-mouse CD11c mAb. CD11c-positive cells were isolated using an EasySep PE Positive Selection Kit (STEMCELL Technologies) following the manufacturer's instructions. Enriched CD11c-positive cells were gated as LysoDC, Tim-4$^-$ LysoMac, and Tim-4$^+$ LysoMac and sorted using the BD FACSAria™ II Cell Sorter (BD Biosciences). Total RNA was isolated from the sorted cells using an RNeasy Mini Kit (QIAGEN) following the manufacturer's instructions. Next, cDNA was prepared using a ReverTra Ace® qPCR RT Kit (TOYOBO). Quantitative PCR was performed using PowerTrack SYBR Green Master Mix (Applied Biosystems) at 95°C for 10 min followed by 50 cycles at 95°C for 15 s, and at 68°C for 60 s. The PCR primer sets were as follows: *Gpr31b*, 5′-CTCATCTCCTTCTGCAACAGTTGC-3′ and 5′-GTGAGGCTGCCAGCGATGTC-3′; *Gapdh*, 5′-TGGCAAAGTGGAGATTGTTGCC-3′ and 5′-AAGATGGTGATGGGCTTCCCG-3′.

Reanalysis of single-cell RNA sequencing (RNA-seq) data

Single-cell RNA-seq data of PP CD11c$^+$ MHC class II$^+$ cell populations (GSE165040)[23] were downloaded and analyzed using Seurat (version 5.1.0) in R-studio. The filtering criteria were set to include cells with > 200 and < 5,000 genes as well as < 5% mitochondrial reads. The data were normalized and scaled using Seurat functions (NormalizeData and ScaleData). Variable features were identified using the vst method in the FindVariableFeatures function with nfeatures set to 2,000, and were used to compute the principal component analyses using RunPCA. K-nearest and shared nearest-neighbor analyses were computed using FindNeighbors with 10 dimensions. Graph-based clustering was conducted using the Louvain algorithm in the FindClusters function with the resolution set at 0.5 (informed by clustertree, produced by Clustree). RunUMAP was used to visualize the clusters. FeaturePlot was used to visualize the *Gpr31b* or PP phagocyte marker-expressing cells in the clusters.

Two-photon microscopy

The *Gpr31b$^{+/+}$ Cx3cr1$^{gfp/+}$* and *Gpr31b$^{-/-}$ Cx3cr1$^{gfp/+}$* mice were orally administered 50 mM sodium pyruvate via drinking water for 2 weeks. PPs were then collected from the mice and washed with PBS. PPs were fixed with 4% paraformaldehyde for 2 h on ice before being incubated with anti-mouse GP2 mAb. PPs were then incubated in a ScaleS4D25 solution overnight at room temperature to clear the tissue.[38] Images were acquired using an inverted two-photon microscope (A1R-MP; Nikon) equipped with a 20× water immersion lens (Plan Fluor, numerical aperture 0.75; Nikon) and Chameleon Vision II Ti: sapphire laser (Coherent) set at 880 nm for two-photon excitation. The typical optimal *z*-step size was 0.50–1 µm. Serial 50–100 µm *z*-scan images were collected and reconstructed using arivis Vision4D software (version 3.4; ZEISS). The number of dendrites that entered more than one-third of the M cell was then quantified. Additionally, the FAE area was quantified using ImageJ

software (https://imagej.nih.gov/ij/) and the number of dendrite protrusions per FAE area was calculated.

Bacterial titers in PPs and the ileum

Mice were orally administered 5×10^9 colony-forming units (CFU) of *L. monocytogenes* EGDe strain. Four days after infection, PPs and the ileum were collected and washed with PBS. To remove *L. monocytogenes* in the luminal surface, tissue was treated in Dulbecco's Modified Eagle Medium supplemented with 100 µg/mL gentamicin at room temperature for 1 h. After being washed with PBS, the tissue was homogenized and plated on brain heart infusion agar. Colonies were counted 1 day after incubation at 37°C. To compare EGDe and 10403S, mice were administered antibiotics (oral administration of streptomycin, 20 mg/mouse, and intraperitoneal injection of clindamycin, 200 µg/mouse) for 2 consecutive days before *L. monocytogenes* infection.[39] Antibiotic-treated mice were orally infected with 1×10^{11} CFU of *L. monocytogenes* EGDe and 10403S strains. Four days after infection, PPs and the ileum were collected and CFU was evaluated.

Bacteria uptake by phagocytes in PPs

Mice were orally administered 50 mM sodium pyruvate via drinking water for 2 weeks. Mice were then orally administered 1×10^9 CFU of *L. monocytogenes* EGDe strain. PPs were collected 24 h after infection, and PP cells were prepared and incubated with cell-surface marker mAbs as described in the *Cell preparation* and *Flow cytometry* section. The cells were fixed in phosphate buffer containing 4% paraformaldehyde and permeabilized with PBS containing 0.1% TritonX-100, followed by incubation with anti-*L. monocytogenes* antibody. Flow cytometric analysis was performed using a CytoFLEX.

Lactate and pyruvate measurements

Mice were orally administered 1×10^9 CFU of *L. monocytogenes* EGDe strain. One day after infection, the luminal contents of the LP were homogenized in water and centrifuged at $10,000 \times g$ for 10 min at 4°C. The concentrations of D-lactate, L-lactate, and pyruvate in the supernatants were then measured using a D-lactate colorimetric assay kit, lactate colorimetric assay kit II, and pyruvate assay kit (BioVision), respectively, according to the manufacturer's protocols.

RNA-seq

Mice were orally administered 1×10^9 CFU of *L. monocytogenes* EGDe strain. Two days after infection, LysoDCs (6×10^2 to 1.5×10^3 cells) were sorted using the BD FACSAria II cell sorter and total RNA was isolated using an RNeasy Mini Kit (QIAGEN) following the manufacturer's instructions. RNA quality control was performed using an RNA6000 Pico kit for 2100 Bioanalyzer systems (Agilent). The cDNA library was constructed using a SMART-Seq HT PLUS Kit (TaKaRa Bio) following the manufacturer's protocol. Briefly, RNA was extracted and reverse-transcribed into cDNA using oligo(dT) priming and SMART technology to ensure full-length cDNA synthesis. The cDNA was amplified via PCR and converted into Illumina-compatible sequencing libraries using the integrated library preparation components of the kit. Library quality and concentration were evaluated using the High Sensitivity D1000 ScreenTape System (Agilent) and the Qubit dsDNA HS Assay Kit (Invitrogen), respectively. The libraries were pooled and sequenced using a DNBSEQ-T7 (MGI Tech) system.

Bulk RNA-seq data processing and analysis

Raw RNA-seq reads were trimmed and filtered for quality control using fastp. The clean reads were then mapped to the GRCm39 reference genome using HISAT2, and read counts for each sample were obtained using featureCounts. For the principal component analysis (PCA) and the enrichment analysis for

differentially expressed genes, normalized RNA-seq z-score-transformed data were plotted using ggplot2 and DEseq2 R packages. Data were analyzed using iDEP 0.96 (http://bioinformatics.sdstate.edu/idep96/).

Detection of phagosome acidification and cross-presentation

To fluorescently label the bacteria, 2×10^9 CFU of *L. monocytogenes* EGDe strain was incubated in 100 mM sodium bicarbonate containing 0.5 mM pHrodo Red succinimidyl ester (Invitrogen) or PBS containing saturated FITC for 1 h at room temperature. Mice were then orally administered 1×10^9 CFU of unlabeled *L. monocytogenes* EGDe strain. Two days after infection, PP cells (2×10^6 cells) were prepared. For detection of phagosome acidification, PP cells were incubated with pHrodo Red-conjugated or FITC-conjugated *L. monocytogenes* (2×10^8 CFU) at 37°C with 5% CO_2 for 1 h. For detection of cross-presentation, PP cells were incubated with 5 mg/mL of ovalbumin (OVA), 5 mg/mL of bovine serum albumin (BSA), or 10 μg/mL Alexa Fluor 647-conjugated OVA at 37°C with 5% CO_2 for 6 h. The cells were analyzed by flow cytometry as described in the *Flow cytometry* section.

Migration assay

$Gpr31b^{+/+}$ $Cx3cr1^{gfp/+}$ and $Gpr31b^{-/-}$ $Cx3cr1^{gfp/+}$ mice were orally administered 1×10^9 CFU of *L. monocytogenes* EGDe strain. Two days after infection, PP cells (2×10^6 cells) and CCL19 (50 ng/mL) were placed in the upper and lower chambers of a Transwell (5.0-μm pore size; Corning), respectively. After being incubated for 2.5 h at 37°C with 5% CO_2, the cells in the lower chamber were harvested and incubated with cell-surface marker mAbs. Migrated cells were counted using a CytoFLEX flow cytometer with 6.0-μm Fluoresbrite microspheres (Polysciences, Inc).

Quantification of CX3CR1$^+$ cells in the IFR

$Gpr31b^{+/+}$ $Cx3cr1^{gfp/+}$ and $Gpr31b^{-/-}$ $Cx3cr1^{gfp/+}$ mice were orally administered 1×10^9 CFU of *L. monocytogenes* EGDe strain. Two days after infection, PPs were collected and fixed in phosphate buffer containing 4% paraformaldehyde. Fixed PPs were embedded in O. C. T. compound (Sakura Finetek) and 30-μm frozen sections were cut with a Leica CM1950 cryostat (Leica Biosystems). The sections were then incubated with anti-mouse CD4 mAbs. Immunostaining images were obtained using an inverted confocal microscope (A1R; Nikon). The percentage of CX3CR1$^+$ CD4$^-$ area per IFR unit area was quantified using ImageJ software.

L. monocytogenes-specific T cells in PPs and the LP

To increase the susceptibility of mice to *L. monocytogenes*, we treated them with streptomycin, which predisposes hosts to *L. monocytogenes* infection,[39] before orally inoculating them with the bacteria. Mice were orally administered 20 mg/mouse streptomycin for two days, followed by oral infection with 1×10^{10} CFU of *L. monocytogenes* EGDe strain. Seven days after infection, PPs and the small intestines were collected. Prepared cells were cultured with the MHC class II-restricted *Listeria* peptide listeriolysin $O_{190-201}$ (10 μg/mL)[44] or MHC class I-restricted *Listeria* cell wall surface peptide LMON_0576 (10 μg/mL),[45] and GolgiStop at 37°C with 5% CO_2 for 4 h. Collected cells were then analyzed using flow cytometry.

Photoconversion

$Gpr31b^{+/+}$ KikGR mice and $Gpr31b^{-/-}$ KikGR mice were orally administered 20 mg/mouse streptomycin, followed by oral infection with 1×10^{10} CFU of *L. monocytogenes* EGDe strain. Five days after infection, mice were anesthetized and three ileal PPs were exposed and irradiated with violet light (110 mW/cm^2) for 3 min. Immediately after the surgery, the mouse abdomen was closed with wound clips. Twenty-four hours later, PPs and the small intestine were collected. The cells were prepared and analyzed using flow cytometry as described in the *Cell preparation* and *Flow cytometry* sections.

Resistance to *L. monocytogenes*

Mice were orally administered 50 mM sodium pyruvate via drinking water for 2 weeks. For immunization, mice were orally administered 1×10^9 CFU of *L. monocytogenes* strain EGDe, which selectively invade PPs (Supplementary Figure S2(a)). The oral administration of EGDe did not compromise survival rate. On 12–13 days after immunization, mice were administered antibiotics (oral administration of streptomycin, 20 mg/mouse, and intraperitoneal injection of clindamycin, 200 μg/mouse)[39]. On day 14 after immunization, mice were orally challenged with 1×10^{11} CFU of *L. monocytogenes* strain 10403S, which shows relatively high virulence.[40] Body weight and survival rate were evaluated daily.

Statistical analysis

Statistical analysis was performed using GraphPad Prism 7 (GraphPad Software). Significance was determined using Student's *t*-test or one-way ANOVA followed by the Tukey – Kramer test unless otherwise described. Data are shown as the mean ± standard deviation.

Results

GPR31 is selectively expressed in LysoDCs in PPs

GPR31 is expressed in CX3CR1^{high} cells in the small intesitne.[32] Given that PPs are main inductive sites for intestinal immunity, we speculate that GPR31 is expressed on myeloid cell subset(s) unique to PPs and regulates intestinal immune responses. To identify the population expressing GPR31 in detail, we sorted LysoDCs (CX3CR1^{high} MHC class II^{high} CD4$^-$), Tim-4$^+$ LysoMacs (Tim-4$^+$ CX3CR1^{high} MHC class II^{low} CD4$^+$), and Tim-4$^-$ LysoMacs (Tim-4$^-$ CX3CR1^{high} MHC class II^{low} CD4$^+$)[20] from *Cx3cr1*$^{gfp/+}$ mice (Figure 1(a)). The expression of *Gpr31b* was readily detected in LysoDCs (Figure 1(b)). To further characterize the GPR31-expressing cell population, we reanalyzed a single-cell RNA-seq dataset from a study that reported CD11c$^+$ MHC class II$^+$ cell populations in PPs.[23] In the uniform manifold approximation and projection (UMAP) analysis, *Gpr31b* was mainly detected in cluster 2, which expressed *Cx3cr1* and represented LysoDCs and LysoMacs. In cluster 2, the expression pattern of *Gpr31b* was similar to that of *Emb* (encoding embigin) and *F11r* (JAM-A), which are reportedly expressed in a mature LysoDC subset,[18] whereas it was not associated with that of *Cd4* (Figure 1(c)). We next examined *Gpr31b* expression in LysoDCs of *Gpr31b*$^{+/+}$ *Cx3cr1*$^{gfp/gfp}$ mice because *Gpr31b* expression in CX3CR1$^+$ MNPs in the LP is regulated at the mRNA level by CX3CR1 and its ligand CX3CL1/fractalkine.[32] In PP LysoDCs, *Gpr31b* expression was significantly decreased in *Cx3cr1*$^{gfp/gfp}$ mice (in which *Cx3cr1* locus is replaced by the cDNA encoding EGFP) than in *Cx3cr1*$^{+/+}$ mice (Figure 1(d)). These findings indicate that *Gpr31b* is preferentially expressed in LysoDCs under the control of CX3CR1 signaling in PPs.

Pyruvate and GPR31 promote LysoDC dendrite protrusion into M-cell pockets

LysoDCs reside beneath the FAE and extend their dendrites into basolateral M-cell pockets. To explore whether GPR31 signaling participates in this process, we visualized the interactions between CX3CR1$^+$ cells and M cells in whole PP tissues. We treated PPs with Sca*l*eS, a sorbitol-based optical tissue clearing method that preserves tissue microarchitecture and minimally quenches fluorescent signals,[38] and used two-photon microscopy to achieve optimal spatial resolution. The localization of LysoDCs beneath the FAE was uncompromised by *Gpr31b* deficiency. Dendrite extension by LysoDCs into M-cell pockets was detected in *Gpr31b*$^{+/+}$ *Cx3cr1*$^{gfp/+}$ mice and was significantly decreased in *Gpr31b*$^{-/-}$ *Cx3cr1*$^{gfp/+}$ mice (Figure 2(a,b); Supplementary Video 1, 2). Decreased LysoDC dendrite extension was also observed in *Gpr31b*$^{+/+}$ *Cx3xr1*$^{gfp/gfp}$ mice (Figure 2(a, b); Supplementary Video 3), supporting our observation that CX3CR1 signaling regulated *Gpr31b* transcript expression in LysoDCs (Figure 1(d)). We next orally administered pyruvate to *Gpr31b*$^{+/+}$ *Cx3cr1*$^{gfp/+}$ or *Gpr31b*$^{-/-}$ *Cx3cr1*$^{gfp/+}$ mice for 2 consecutive weeks. Pyruvate administration enhanced the numbers of LysoDCs extending their dendrites into M cells in *Gpr31b*$^{+/+}$ *Cx3cr1*$^{gfp/+}$ but not *Gpr31b*$^{-/-}$ *Cx3cr1*$^{gfp/+}$ mice (Figure 2(a,b); Supplementary Video 4, 5). *Gpr31b* deficiency did not affect the number of M cells per unit area of FAE (Supplementary Figure 1(a)). Notably, the transepithelial
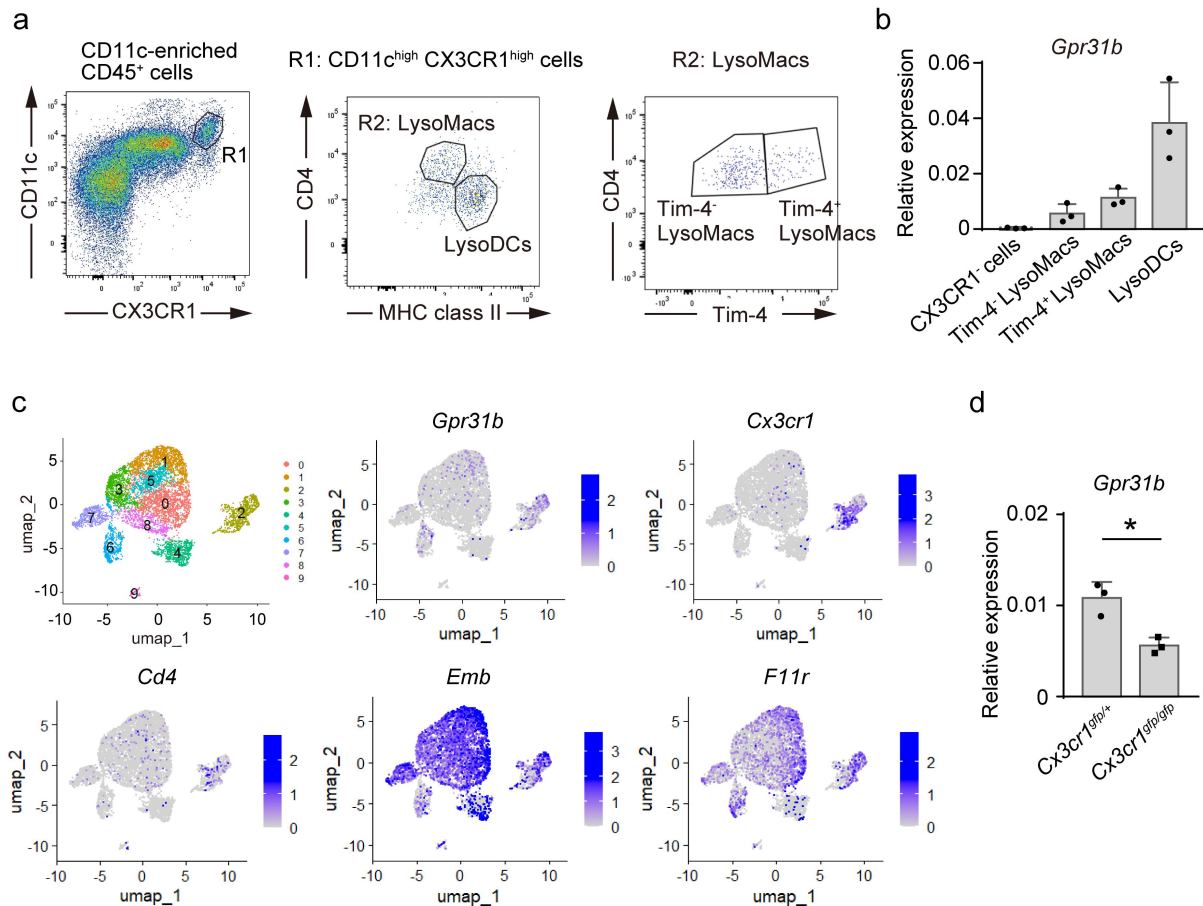
Figure 1. *Gpr31b* is highly expressed in LysoDCs. (a) Gating strategies of MNPs in PPs for cell sorting. Leukocytes were collected from PPs of *Gpr31b*$^{+/+}$ *Cx3cr1*$^{gfp/+}$ mice, and CD11c$^+$ cells were magnetically enriched. The LysoDC and LysoMac subsets were separated by the expression of MHC class II, CD4, and Tim-4. (b) Quantitative PCR analysis of *Gpr31b* in PP phagocytes. Expression levels were normalized to *gapdh* ($n = 3$). (c) UMAP analysis for the expression of *Gpr31b* and PP phagocyte markers in PP CD11c$^+$ MHC class II$^+$ cell populations from a publicly available dataset.[23] (d) *Gpr31b* expression in LysoDCs of *Gpr31b*$^{+/+}$ *Cx3cr1*$^{gfp/gfp}$ mice. (b,d) Data represent the mean ± standard deviation from three mice.

dendrite protrusion that was observed in LP CX3CR1$^+$ MNPs was rarely observed in PPs of *Gpr31b*$^{+/+}$ *Cx3cr1*$^{gfp/+}$ and *Gpr31b*$^{-/-}$ *Cx3cr1*$^{gfp/+}$ mice irrespective of pyruvate administration (Supplementary Figure 1(b)). Although it has been reported that LysoDCs extend trans-M-cell dendrites to the lumen,[43] we only occasionally detected dendrites penetrating the apical surface of M cells irrespective of *Gpr31b* expression. In *Gpr31b*$^{+/+}$ *Cx3cr1*$^{gfp/+}$ mice, LysoDCs normally had elongated finger-like dendrites (Figure 2 (c,d); Supplementary Video 6); however, oral pyruvate administration enhanced the number of LysoDCs forming dendritic processes with spherical ("balloon") shapes (Figure 2(e,f); Supplementary Video 7). These spherical dendrites often occupied M-cell pockets occasionally with leukocytes (Figure 2(e)), which may help to expand the surface area of LysoDCs, thereby allowing them to easily access the antigens delivered by M cells and interact with other leukocytes. Collectively, these observations suggest that pyruvate – GPR31 signaling plays a critical role in LysoDC dendrite protrusion into basolateral M-cell pockets.

Pyruvate – GPR31 signaling promotes pathogenic bacteria uptake by LysoDCs

To investigate whether GPR31 signaling affects pathogen uptake in PPs, we orally inoculated mice with *L. monocytogenes*. In mice, these bacteria are transferred through M cells at PPs but not through the epithelial layer of the small intestine.[8,11–13] In *Gpr31b*$^{+/+}$ mice 4 days after infection, *L. monocytogenes* strain EGDe invaded PPs but not the LP (Supplementary Figure 2(a)). Compared with *Gpr31b*$^{+/+}$ mice, *Gpr31b*$^{-/-}$ mice exhibited a lower burden of *L. monocytogenes* in PPs (Supplementary Figure 2(a)). We next analyzed
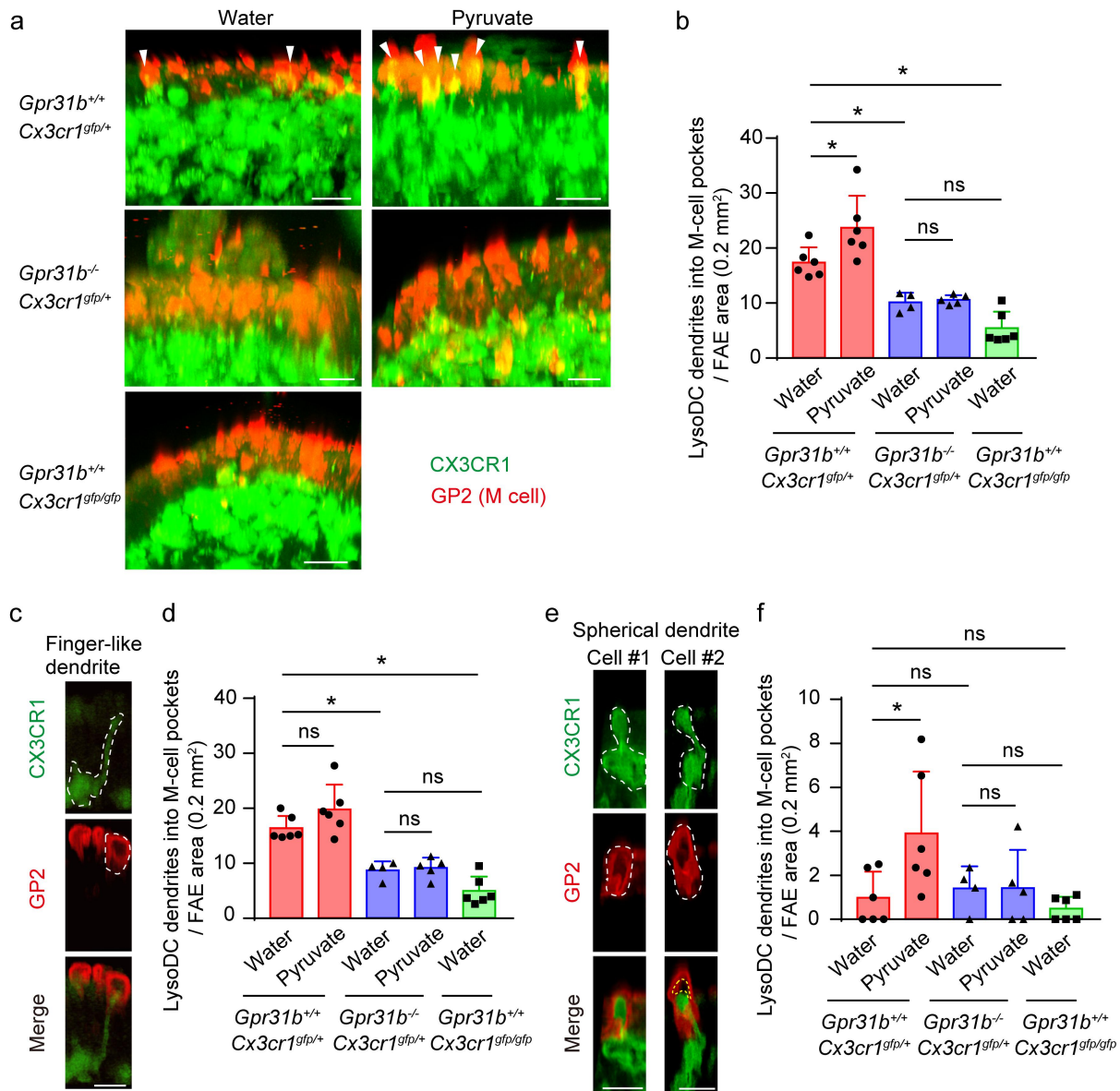
Figure 2. Pyruvate – GPR31 axis enhances dendrite protrusion of LysoDCs into M-cell pockets. (a–f) *Gpr31b*$^{+/+}$ *Cx3cr1*$^{gfp/+}$, *Gpr31b*$^{-/-}$ *Cx3cr1*$^{gfp/+}$, and *Gpr31b*$^{+/+}$ *Cx3cr1*$^{gfp/gfp}$ mice were treated with oral pyruvate administration. PP tissue from each mouse was stained with anti-GP2 mAb (red) and treated with the optical tissue clearing solvent Sca*l*eS4D25. The morphology of CX3CR1^{+} cell dendrites (green) in PPs were observed using two-photon microscopy. Arrowheads indicate CX3CR1^{+} cell dendrites protruding into M-cell pockets (a). Total dendrites in M-cell pockets (b), finger-like dendrites in M-cell pockets (d), and spherical dendrites in M-cell pockets (f) per FAE area. (c,e) volume rendering-based 3D reconstruction of LysoDCs with a finger-like dendrite (c) or a spherical dendrite (e). The white line delineates a single CX3CR1^{+} cell or M cell. The yellow line indicates a leukocyte in a M-cell pocket as judged by the autofluorescence. Bars in (a, c, and e) represent 20 μm. Each symbol represents an individual PP (*n* = 4–7 tissues from three mice). Data represent the mean ± standard deviation. *$p < 0.05$, ns: not significant.

the phagocyte populations actively involved in bacteria uptake. In *Gpr31b*$^{+/+}$ mice, LysoDCs took up the pathogen more efficiently than LysoMacs or conventional DCs (cDCs) (Figure 3(a,b)). Notably, bacteria uptake by LysoDCs was significantly decreased in *Gpr31b*$^{-/-}$ mice than in *Gpr31b*$^{+/+}$ mice (Figure 3(a,b)). Furthermore, oral pyruvate administration significantly enhanced bacteria uptake by LysoDCs in *Gpr31b*$^{+/+}$ but not *Gpr31b*$^{-/-}$ mice (Figure 3(a,b)). The luminal production levels of pyruvate, D-lactate, and L-lactate were similar between uninfected and infected mice, indicating that *L. monocytogenes*-derived GPR31-reactive metabolites have minimal effects on GPR31-dependent bacteria uptake (Supplementary Figure
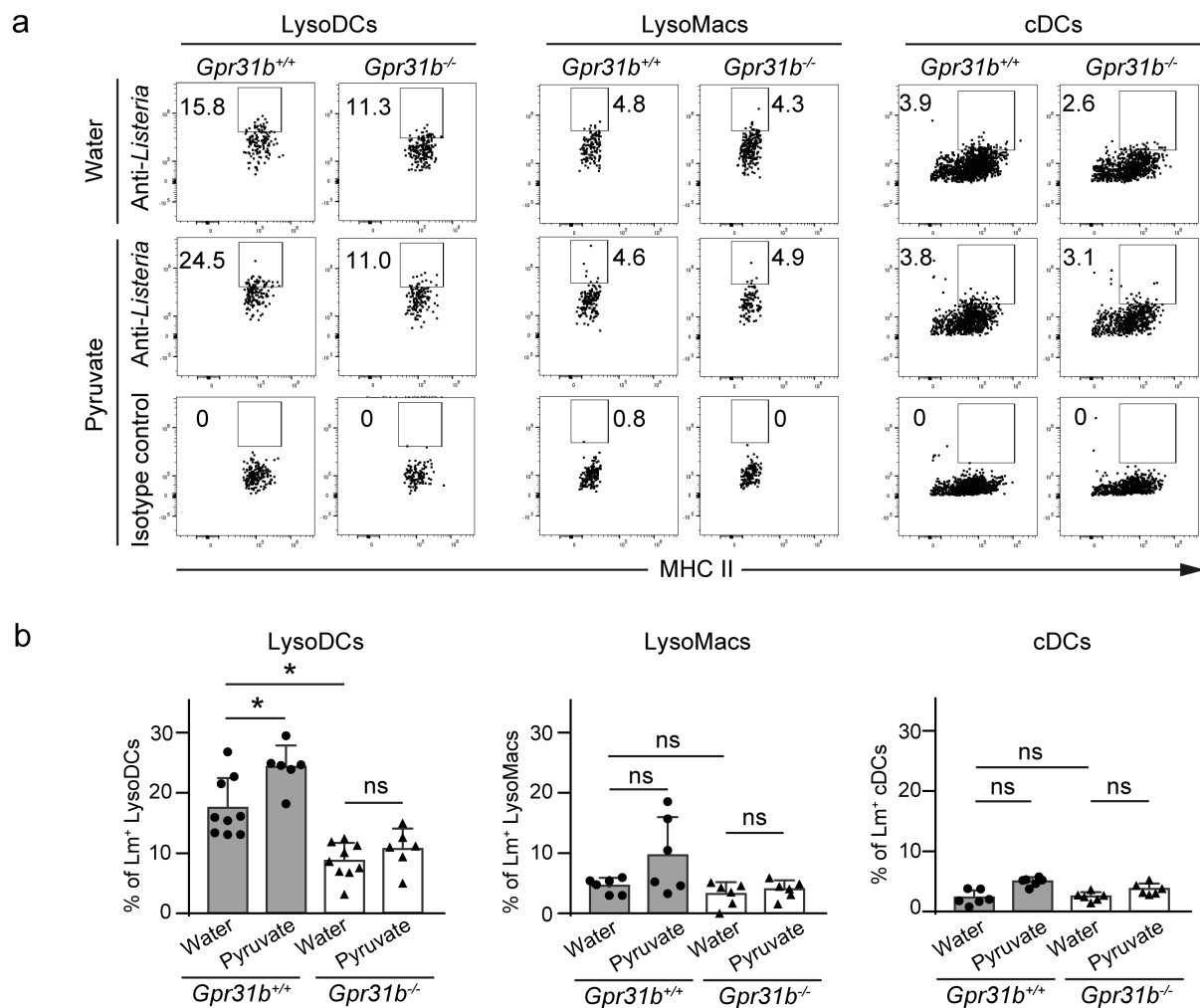
Figure 3. Pyruvate–GPR31 signaling enhances *L. monocytogenes* uptake by LysoDCs. (a and b) *L. monocytogenes* uptake by PP phagocytes. *Gpr31b*^{+/+} or *Gpr31b*^{−/−} mice were orally infected with 1×10^9 CFU of *L. monocytogenes* EGDe strain. Representative dot plot (a) and the percentage (b) of *L. monocytogenes*[+] LysoDCs (left), LysoMacs (middle), and cDCs (right) at 1 dpi (water, *n* = 9 mice; pyruvate,*n* = 6 mice). *$P < 0.05$. ns: not significant.

S2(b)). Collectively, these findings suggest that the pyruvate – GPR31 axis positively regulates pathogenic bacteria uptake by LysoDCs.

GPR31 signaling enhances antigen processing in LysoDCs

We next assessed whether GPR31 signaling alters global transcriptional changes in LysoDCs upon infection. We isolated LysoDCs from *Gpr31b*^{+/+} mice and *Gpr31b*^{−/−} mice with or without *L. monocytogenes* infection and performed RNA-seq on these cells. Principal component analysis (PCA) revealed a distinct separation between *Gpr31*^{+/+} LysoDCs and *Gpr31b*^{−/−} LysoDCs with or without infection (Figure 4(a)). Under infection conditions, differentially expressed genes in *Gpr31b*^{−/−} mice were associated with cell activation, leukocyte activation, and lymphocyte activation (Figure 4(b), Table S1). Mapping of the differentially expressed genes to the Kyoto Encyclopedia of Genes and Genomes database returned several genes associated with antigen processing and presentation. These genes have been ascribed to proton pumps for acidification of the phagosome – such as *Atp6v0c* and *Atp6v0a1*, which encode subunits of vacuolar ATPase – and proteases that are necessary for the processing of antigens and invariant chains, such as *Lgmn* (legumain/asparaginyl endopeptidase), *Ctsb* (cathepsin B), and *Ctsd* (cathepsin D) (Figure 4(c)).

We next tested whether GPR31 signaling indeed regulates antigen processing. Given that the difference of gene expression associated with antigen processing was more distinguished under infected conditions, we
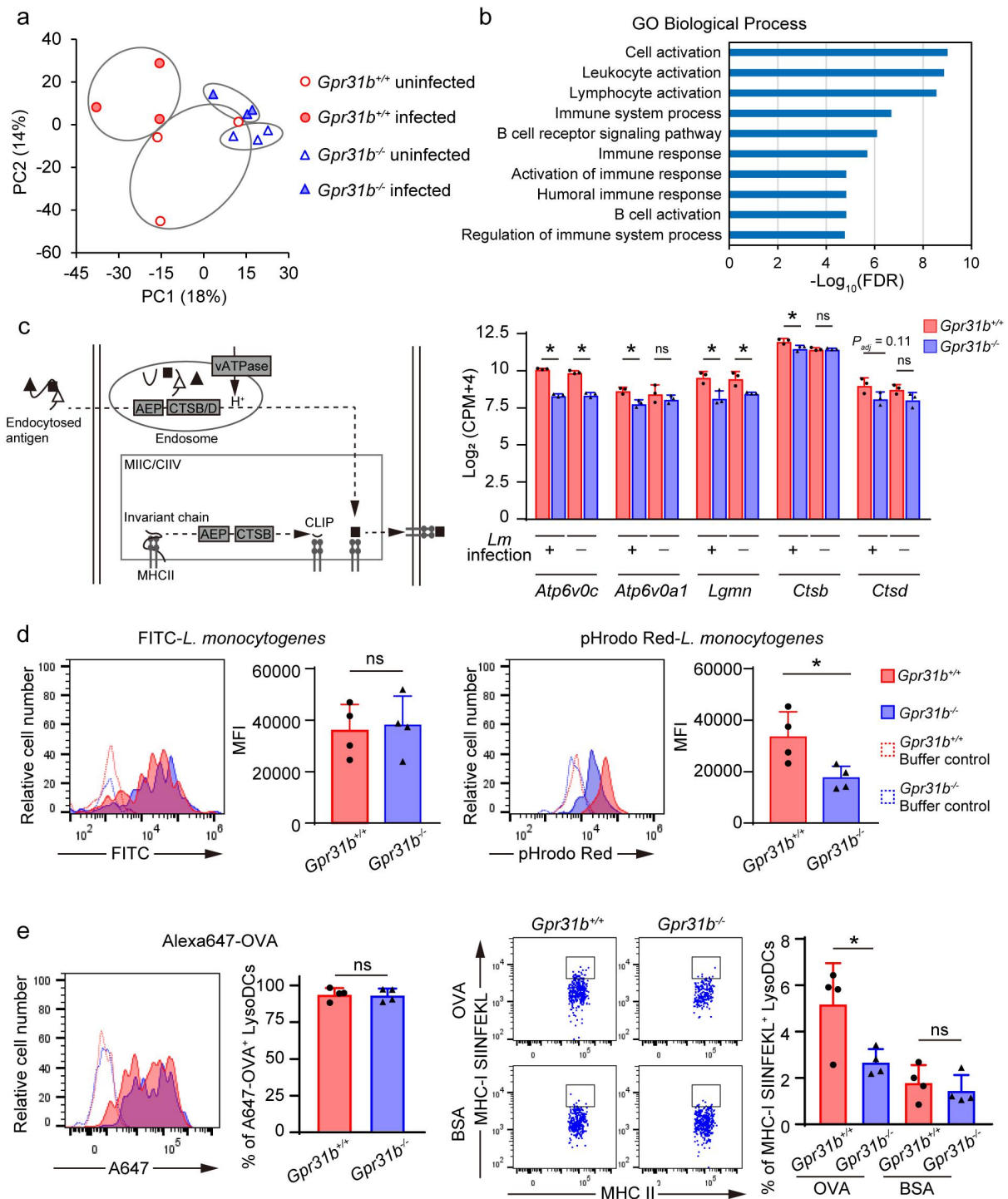
Figure 4. GPR31 signaling enhances bacterial antigen processing with altered gene expression profiles. (a–c) RNA-seq analysis of LysoDCs, sorted from $Gpr31b^{+/+}$ and $Gpr31b^{-/-}$ mice with or without *L. monocytogenes* infection at 2 dpi (1×10^9 CFU/mice; $n = 3$ mice). (a) Principal component (PC) analysis. (b) Enriched gene ontology (GO) biological process terms between $Gpr31b^{+/+}$ and $Gpr31b^{-/-}$ mice upon infection. (c) Differentially expressed genes mapped to antigen processing and presentation in Kyoto encyclopedia of genes and genomes (KEGG) pathways (left) and their expression in $Gpr31b^{-/-}$ LysoDCs is shown (right). Log_2 Fold changes with p-adjusted value ($Padj$) < 0.1 were considered significant. (d) Phagosome acidification activity of LysoDCs. PP cells from *L. monocytogenes*-infected $Gpr31b^{+/+}$ or $Gpr31b^{-/-}$ mice at 2 dpi (1×10^9 CFU/mice; $n = 4$ mice) were incubated with FITC or pHrodo Red -conjugated *L. monocytogenes* for 1 h. The mean fluorescence intensities (MFI) of FITC and pHrodo Red were measured using flow cytometry. (e) PP cells from *L. monocytogenes*-infected $Gpr31b^{+/+}$ or $Gpr31b^{-/-}$ mice at 2 dpi (1×10^9 CFU/mice; $n = 4$ mice) were incubated with Alexa Fluor 647-conjugated OVA, unlabeled-OVA, or BSA for 6 h. Frequencies of LysoDCs positive for Alexa Fluor 647 or MHC-I SIINFEKL peptide-loading complex were measured using flow cytometry. *p < 0.05, ns: not significant.

first prepared LysoDCs from *Listeria*-infected *Gpr31b*^{+/+} and *Gpr31b*^{-/-} mice. The cells were then cultured *in vitro* with *L. monocytogenes* labeled with FITC or the pH-sensitive dye pHrodo[TM] Red, which has low fluorescence at neutral pH and bright fluorescence at acidic pH, to monitor the acidification of bacteria-containing phagolysosomes. The *Gpr31b*^{+/+} and *Gpr31b*^{-/-} LysoDCs had similar capacities for bacterial engulfment as assessed by the uptake of FITC-labeled bacteria (Figure 4(d)). However, *Gpr31b*^{-/-} LysoDCs had weaker fluorescence than *Gpr31b*^{+/+} LysoDCs in pHrodo-labeled bacteria (Figure 4(d)), indicating that the phagolysosomes of *Gpr31b*^{-/-} LysoDCs are not fully acidified. It has been reported that LysoDCs elicit cross-presentation to prime antigen-specific CD8^{+} T cells.[23] To examine whether GPR31 signaling promotes MHC class I-loaded antigen peptide formation, we treated LysoDCs with soluble OVA protein and evaluated SIINFEKL peptide bound to H-2K[b] of MHC class I on the cell surface. Whereas *Gpr31b*^{-/-} LysoDCs underwent phagocytosis of OVA to a comparable level to their *Gpr31b*^{+/+} counterparts *in vitro*, they showed the significantly decreased formation of MHC class I-loaded SIINFEKL peptide (Figure 4(e)). Together, our findings suggest that GPR31 signaling directly enhances bacterial antigen processing by LysoDCs, in addition to inducing dendrite formation.

GPR31-dependent antigen sampling promotes LysoDC migration to the IFR

CD11b^{+} DCs or LysoDCs localized in the SED migrate to the T cell-enriched IFR upon stimulation with *Toxoplasma gondii* tachyzoite antigen and the TLR7/8 agonist R848,[18,25] with the upregulation of CCR7 expression at the cell surface.[18] CCL19, a functional ligand of CCR7, is predominantly expressed in fibroblastic reticular cells in the IFR in secondary lymphoid organs.[42] A CXCR4 ligand, CXCL12, is also abundant in the IFR as well as in the subserosal region of PPs.[43] We next evaluated whether GPR31 signaling is involved in LysoDC migration in PPs. In *Gpr31b*^{+/+} mice, *L. monocytogenes* infection increased the proportion of LysoDCs bound to CCL19 or CXCL12, and this binding was significantly suppressed by *Gpr31b* deficiency (Figure 5(a)). Functionally, *Gpr31b*^{-/-} LysoDCs exhibited poorer migration toward CCL19 than their *Gpr31b*^{+/+} counterparts (Figure 5(b)). Additionally, *Gpr31b*^{-/-} *Cx3cr1*[gfp/+] mice showed fewer LysoDCs in the IFR than *Gpr31*^{+/+} *Cx3cr1*[gfp/+] mice 2 days after infection (Figure 5(c)). These findings suggest that the GPR31 signaling-dependent sampling of pathogenic bacteria facilitates LysoDC migration from the SED to the IFR.

GPR31-dependent antigen sampling enhances Th1 and cytotoxic T cell responses to *L. monocytogenes*

LysoDCs have been reported to prime naïve T cells toward Th1 as well as cytotoxic T cells.[20,23] We next interrogated whether GPR31-dependent antigen capture by LysoDCs promotes effector T cell responses. Upon *L. monocytogenes* infection, *Gpr31b*^{-/-} mice exhibited a decreased proportion of LysoDCs expressing the costimulatory molecule CD86 but not CD40 or CD80 (Supplementary Figure S3). Seven days after inoculation, we secondarily stimulated PP or LP cells with H-2[b]-restricted listeriolysin O peptide[40] to evaluate antigen-specific Th responses. The proportion of *L. monocytogenes*-specific T cells producing IFN-γ was significantly lower in *Gpr31b*^{-/-} mice than *Gpr31b*^{+/+} mice in both PPs and the LP (Figure 6(a)). By contrast, the proportion of those producing IL-17 was similar between *Gpr31b*^{+/+} mice and *Gpr31b*^{-/-} mice. We also examined the involvement of GPR31 signaling in antigen-specific cytotoxic T cell responses by stimulating PP or LP cells with H-2[b]-restricted *Listeria* cell wall surface peptide, which activates CD8^{+} T cells.[41] As depicted in Figure 6(b), *Gpr31b*^{-/-} mice showed the reduced proportion of pathogen-specific cytotoxic T cells producing IFN-γ in these tissues. These findings indicate that GPR31 signaling enhances T cell priming toward Th1 cells and cytotoxic T cells during *L. monocytogenes* infection.

Effector T cells generated in PPs (inductive sites) enter circulation through the efferent lymphatics and blood vessels before migrating to the LP (effector sites). To examine whether GPR31 signaling is responsible for effector T cell migration from PPs to the LP, we used KikGR mice. These mice express the photoconvertible protein KikGR, which irreversibly changes from green to red upon exposure to violet light, thereby allowing the tracking of cells in the original site.[34] The PPs of *Gpr31b*^{+/+} KikGR mice and *Gpr31b*^{-/-} KikGR mice were exposed to violet light 5 days after the oral inoculation of *L. monocytogenes*, and KikGR-Red^{+} (photoconverted) T cells in the LP were monitored the following day. KikGR-Red^{+} effector CD4^{+} and
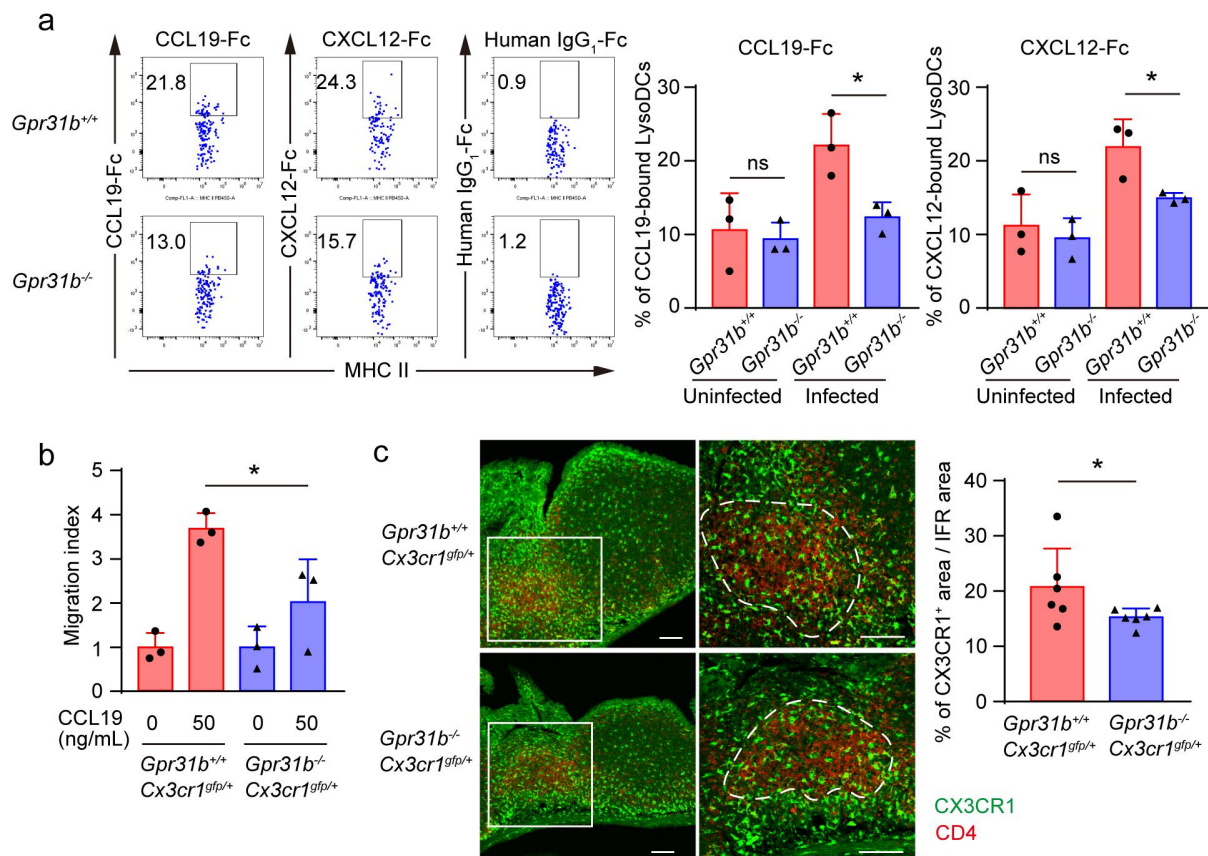
Figure 5. GPR31 signaling enhances LysoDC migration to the IFR in PPs. (a) Chemokine binding of LysoDCs. Mice were orally infected with 1×10^9 CFU of *L. monocytogenes* EGDe strain ($n = 3$ mice). PP LysoDCs were analyzed for CCL19 and CXCL12 binding at 2 dpi. (b) Chemotactic responses of LysoDCs to CCL19. PP cells prepared from *Gpr31b$^{+/+}$ Cx3cr1$^{gfp/+}$* or *Gpr31b$^{-/-}$Cx3cr1$^{gfp/+}$* mice were applied to the upper wells of Transwells, and LysoDC migration toward CCL19 was evaluated using flow cytometry ($n = 3$ wells). (c) Quantification of CX3CR1$^+$ cells in the IFR of PPs collected from *Gpr31b$^{+/+}$ Cx3cr1$^{gfp/+}$* or *Gpr31b$^{-/-}$ Cx3cr1$^{gfp/+}$* mice. The percentage of CX3CR1$^+$ area (green) per IFR area (dashed line) was quantified using image processing software. The IFR area was defined as the CD4$^+$ area (red). Higher magnification views within the square of the left panels are shown in the right panels. Each symbol represents an individual section ($n = 6$ sections from three mice). Bars represent 100 μm. *$p < 0.05$, ns: not significant.

CD8$^+$ T cells were augmented in PPs by *Gpr31b* deficiency, suggesting that they are retained within PPs. By contrast, significantly fewer photoconverted T cells were observed in the LP of *Gpr31b$^{-/-}$* mice (Figure 6(c)). Collectively, our findings indicate that GPR31-dependent signaling in LysoDCs enhances antigen-specific Th1 cell responses to *L. monocytogenes* in PPs and the migration of effector T cells to the LP.

GPR31 signaling enhances resistance to L. monocytogenes infection

We investigated the physiological effects of the pyruvate – GPR31 axis on the resistance of mice to oral *L. monocytogenes* infection. The *Gpr31b$^{-/-}$* mice were generated on a C57BL/6 background. Although this mouse strain is highly resistant to orally administered *L. monocytogenes*,[46] the susceptibility depends on the bacteria strain. Among the commonly used strains in laboratories, 10403S reportedly shows relatively high virulence.[40] We therefore compared the bacterial burden between the 10403S and EGDe strains. EGDe exclusively invaded the small intestine via PPs, whereas 10403S was detected in the LP 4 days after oral inoculation (Figure 7(a)). *Gpr31b$^{+/+}$* mice inoculated with 10403S consistently showed a marked loss of body weight compared with those received EGDe (Figure 7(b)), indicating that the 10403S strain is highly invasive into the LP, thereby increasing susceptibility.

We next treated mice with or without pyruvate for 2 weeks and immunized them with the EGDe strain to induce immune responses in PPs. Two weeks after the immunization, the mice were orally infected with the
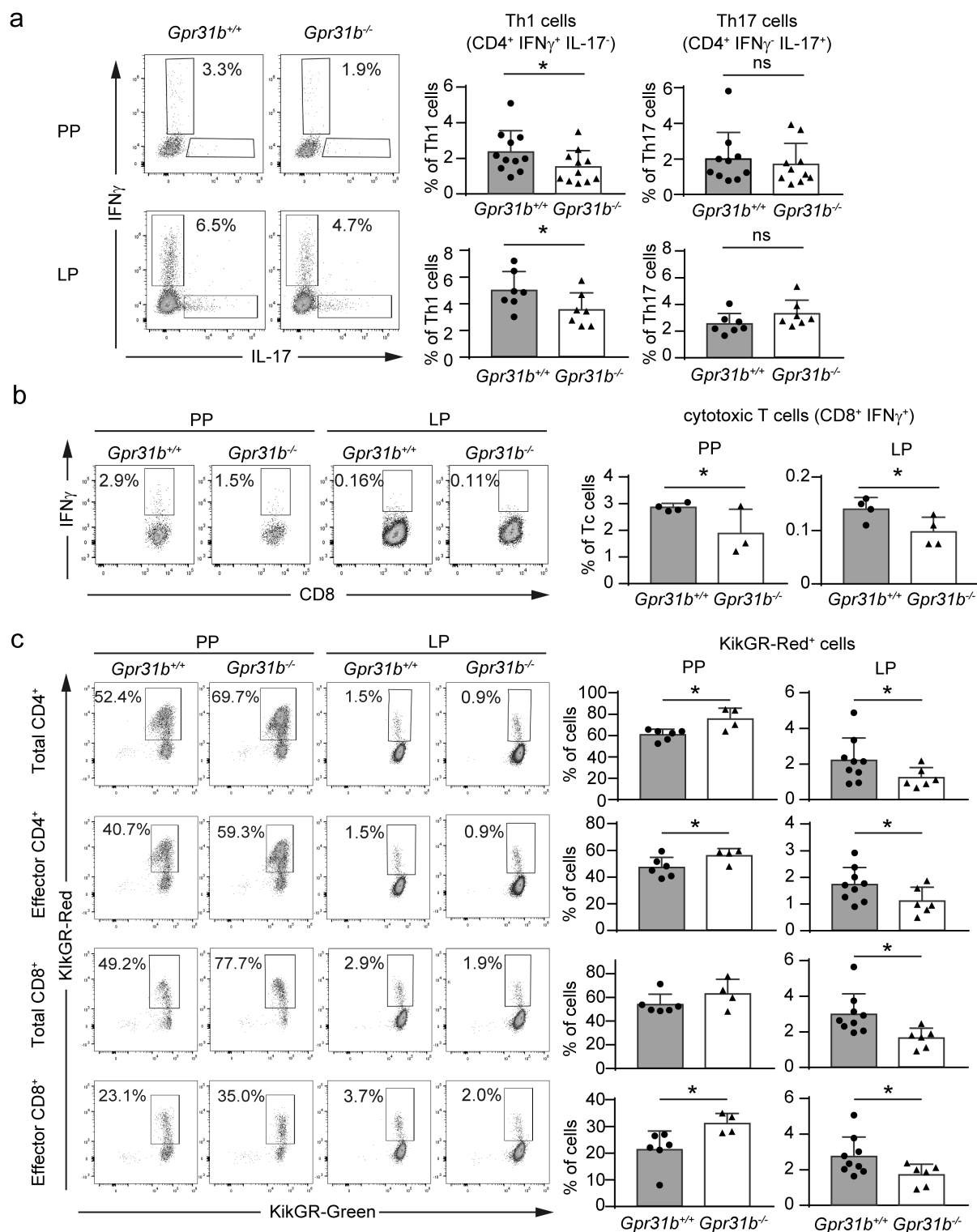
Figure 6. GPR31 signaling enhances T cell responses to *L. monocytogenes* in PPs and the LP. (a and b) frequency of *L. monocytogenes*-specific T cell populations in PPs and the LP from *Gpr31b*$^{+/+}$ or *Gpr31*$^{-/-}$ mice at 7 dpi. PP and LP cells were secondarily stimulated with *L. monocytogenes* listeriolysin O$_{190-201}$ peptide (a) or cell wall surface peptide LMON_0576 (b) *in vitro*. CD4$^+$ cells producing IFN-γ or IL-17 ((a); PP, *n* = 11 mice; LP, *n* = 7 mice) and CD8$^+$ cells producing IFN-γ ((b); PP, *n* = 3–4 mice; LP, *n* = 4 mice) were analyzed. (c) T cell migration from PPs to the LP after *L. monocytogenes* infection. PPs of *Gpr31b*$^{+/+}$ KikGR mice (*n* = 9) and *Gpr31b*$^{-/-}$ KikGR mice (*n* = 6) were labeled using violet light irradiation at 5 dpi. One day after photoconversion, KikGR-Red$^+$ T cells in PPs and the LP were analyzed using flow cytometry. Effector CD4/CD8$^+$ T cell populations were gated as TCRβ$^+$ CD62L$^-$ CD44$^+$ cells. *p < 0.05, ns: not significant.
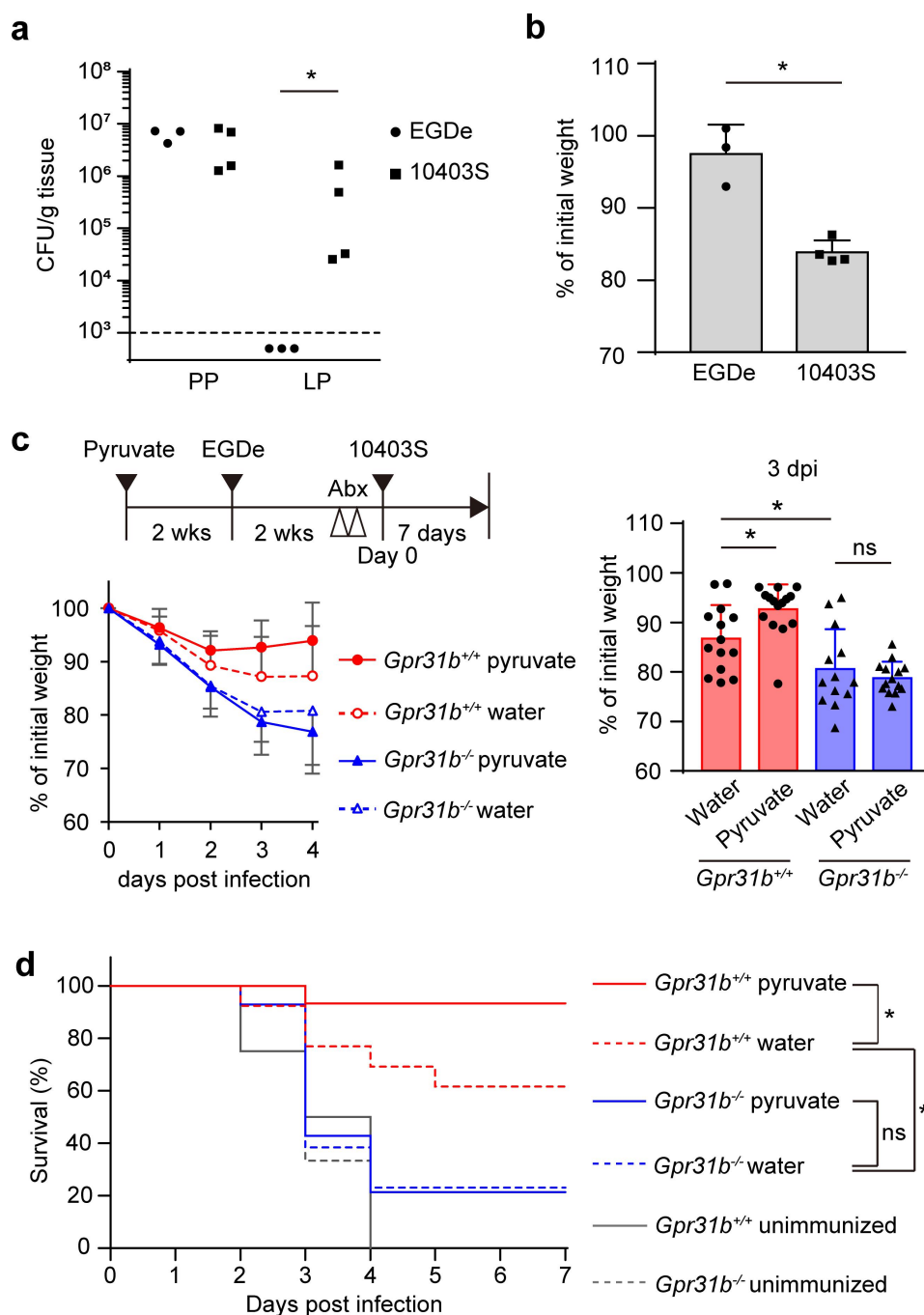
Figure 7. GPR31 signaling enhances resistance to *L. monocytogenes* infection. (a and b) titers of EGDe and 10403S strains in PPs and the LP (a) and body weight loss of *Gpr31b*^{+/+} mice infected with each strain (b) at 4 dpi (1×10^{11} CFU/mice; EGDe, *n* = 3 mice; 10403S, *n* = 4 mice). The dashed line in (a) indicates the detection limit. Mann–Whitney *U*-test (a) was performed for the statistical analysis. (c and d) effects of immunization with the EGDe strain on infection with the invasive 10403S strain. Mice were orally administered pyruvate for 2 weeks before being infected with the EGDe strain (1×10^9 CFU/mice). Two weeks later, mice were further treated with the 10403S strain (1×10^{11} CFU/mice). Body weight loss (c) and survival rate (d) after 10403S infection were monitored (*n* = 13–15 mice). Abx; streptomycin and clindamycin. Log-rank test (d) was performed for statistical analysis. *$p < 0.05$, ns: not significant.

invasive 10403S strain. Without pyruvate treatment, *Gpr31b*^{-/-} mice exhibited a severe loss of body weight compared with *Gpr31b*^{+/+} mice. Oral pyruvate administration alleviated the body weight loss in *Gpr31b*^{+/+} but not *Gpr31b*^{-/-} mice (Figure 7(c)). Consistent with this finding, *Gpr31b*^{-/-} mice were highly susceptible to 10403S and succumbed to the infection shortly after inoculation. Although pyruvate treatment improved

the survival rate in *Gpr31b*^{+/+} mice, this effect was abolished by *Gpr31b* deficiency (Figure 7(d)). These data strongly suggest that the pyruvate – GPR31 axis enhances immune responses in PPs and potentiates the resistance to invasive pathogens in the intestine.

Discussion

LysoDCs reside under the FAE and are closely associated with M cells in PPs. They effectively capture pathogenic bacteria and induce antigen-specific immune responses. In the present study, the bacterial metabolite pyruvate enhanced LysoDC dendrite protrusion to basolateral M-cell pockets via GPR31. Moreover, GPR31 signaling promoted the LysoDC uptake and antigen processing of orally infected *L. monocytogenes*. Upon infection, GPR31 signaling increased both LysoDC migration to the IFR and the generation of antigen-specific Th1 and cytotoxic T cells in PPs, leading to efficient effector T cell migration from PPs to the LP. Furthermore, oral pyruvate administration in mice improved their resistance to infection with a virulent strain of *L. monocytogenes* in a GPR31-dependent manner.

In the current study, we observed that LysoDCs extended dendrites into M-cell pockets but only marginally extended them between adjacent epithelial cells of the FAE. By contrast, CX3CR1[+] MNPs in the LP reportedly protrude transepithelial dendrites in a GPR31-dependent manner.[32] One possible reason for this discrepancy involves the different intrinsic properties of these two cell populations. In the intestinal villi, adjacent epithelial cells form a junctional complex including tight junctions, adherens junctions, and desmosomes, which restrict CX3CR1[+] MNPs from protruding dendrites to the luminal surface. *In vitro* data indicates that DCs open the tight junctions between epithelial cells and extend dendrites outside the epithelial layer without disrupting the tight junctions.[47,48] LP CX3CR1[+] MNPs may have molecular devices that modulate adhesive interactions with epithelial cells for their dendrite protrusion, unlike LysoDCs. Another possibility is that the microenvironment may influence dendrite formation. With maturation, M cells structurally develop basolateral pockets,[2] which generate enough space for LysoDCs to easily elongate dendrites. In addition, the epithelial cells of the FAE covering PPs show specialized characteristics that are distinct from those of intestinal epithelial cells.[49] Although IL-22 regulates the barrier function of intestinal epithelial cells, IL-22 signaling in the FAE is ameliorated by the action of IL-22-binding protein (IL-22BP/IL-22Ra2), which is a secreted decoy receptor for IL-22.[50] IL-22BP alters the transcriptional program of the FAE and promotes bacteria uptake into PPs.[50] Notably, IL22BP is highly expressed by LysoDCs[16,23] under the control of transcription factor RelB and C/EBPα,[51] indicating that LysoDCs may modulate epithelial functions that are important for antigen transport into PPs. Likewise, TLR2 activation induces receptor redistribution in the FAE but not in villus epithelium, and enhances the transepithelial transport of microparticles by M cells.[52] Thus, the FAE might support M cell-mediated antigen transport instead of restricting transepithelial dendrites by LysoDCs. In the intestinal villi, TLR ligands including peptidoglycan, lipopolysaccharide, and CpGs (activating TLR2, TLR4, and TLR9, respectively) enhance CX3CR1[+] MNP dendrite extension into the lumen; however, these ligands fail to induce dendrite formation in bone marrow chimeric mice in which *Myd88*-deficinet recipients received WT hematopoietic cells, indicating the importance of MyD88-dependent TLR signaling in epithelial cells for transepithelial dendrite extension.[53] Further investigations are needed to reveal the mechanisms by which epithelial cells regulate CX3CR1[+] cell dendrite protrusion.

In the present study, oral pyruvate administration particularly enhanced LysoDC dendrites with spherical ("balloon") shapes in a GPR31-dependent manner. This dendrite structure may help to expand the surface area of LysoDCs to promote the efficient uptake of antigens delivered by M cells. This observation is similar to a previous finding that CX3CR1[+] MNPs in the LP display transepithelial dendrites with balloon shapes, especially in the proximal jejunum.[53] Unlike LP CX3CR1[+] MNPs, LysoDCs need to adjust their dendrites to the space of M-cell pockets. It remains unclear whether GPR31 signaling intrinsically induces a spherical dendritic shape, or whether it induces the elongation of finger-like dendrites that subsequently change their shapes to fill the limited space of M-cell pockets. LysoDCs also reportedly extend dendrites through M-cell-specific transcellular pores to the lumen in a CX3CR1-independent manner;[20,41] however, this type of dendrite formation was only occasionally observed in our analysis. Although the reason for this inconsistency is unclear, one possibility is that trans-M cell dendrite formation is dependent on the intestinal environment, including food and intestinal bacteria. It has recently been reported that short-

chain fatty acids induce dendrite elongation in DCs *in vitro* by inhibiting histone deacetylase.[54] It may therefore be that multiple mechanisms regulating dendrite protrusion in DCs are used depending on the biological context.

Although both LysoDCs and cDC2s reside in the SED,[16] LysoDCs play a pivotal role in the uptake of pathogenic bacteria, including *S.* Typhimurium.[21] In the current study, we demonstrated that LysoDCs efficiently took up *L. monocytogenes* in a GPR31-dependent manner using an *L. monocytogenes* strain that preferentially invades PPs. GPR31 signaling promoted *L. monocytogenes* uptake in LysoDCs *in vivo*, whereas *in vitro* experiments revealed that *Gpr31b*⁻/⁻ LysoDCs have a similar capacity for bacteria engulfment as their *Gpr31b*⁺/⁺ counterparts, indicating that the relatively low LysoDC bacteria uptake in *Gpr31b*⁻/⁻ mice may be caused by limited dendrite formation. Moreover, cultured *Gpr31b*⁻/⁻ LysoDCs exhibited low acidification in bacteria-containing phagosomes, indicating that GPR31 signaling directly regulates LysoDC bacteria processing as well as the induction of dendrite protrusion in these cells. cDCs expressing *Zbtb46* enter M-cell pockets and cDC1s mainly participate in the uptake of CpG-carrying nanoparticles,[55] whereas CX3CR1⁺ cells in the SED efficiently take up microspheres, IgA-coated antigens, M cell-derived vesicles, and dead M cells.[20,21,56,57] The involvement of GPR31 signaling in the uptake and processing of these antigens requires further investigation.

LysoDCs strongly express MHC class II and have functional plasticity for the differentiation of naïve helper T cells producing IFN-γ and IL-17.[20,22] In our data, GPR31 signaling promoted *L. monocytogenes*-specific Th1 but not Th17 cell responses, probably because *L. monocytogenes* favors the differentiation and growth of Th1 cells.[58] Upon *L. monocytogenes* infection, PP-resident CX3CR1^intermediate cells but not CX3CR1^high cells (including LysoDCs) are increased in number and serve as main producers of IL-23, which regulates epithelial proliferation.[59] These CX3CR1-expressing myeloid cells may cooperate in the host defense against *L. monocytogenes* infection. The absence of M cells due to the defect of *spib* or diminished transportation of FimH⁺ bacteria in M cells by the deficiency of GP2 leads to the impairment of antigen-specific CD4⁺ T cell responses to *S.* Typhimurium.[4,27] In addition, dysfunction of transcytosis in M cells by the deficiency of allograft inflammatory factor 1 reduces antigen-specific secretory IgA to *Y. enterocolitica*.[60] Therefore, it is tempting to speculate that GPR31 signaling in LysoDCs contributes to immune induction against various pathogens that utilize M cells for entry.

In this present study, we demonstrated the physiological importance of PP LysoDCs for Th1 and cytotoxic T cell induction in not only PPs but also the LP using the *L. monocytogenes* strain EGDe, which preferentially invades PPs but not the LP. Upon infection, GPR31 signaling promoted the migration of effector T cells from PPs to the LP. Furthermore, immunization with the EGDe strain enhanced resistance to the LP-invasive strain 10403S in a GPR31-dependent manner. Together, these findings indicate that immune induction via GPR31 in PPs (the inductive site) plays a fundamental role in the host defense against pathogenic bacteria in the effector site. It has also been reported that M cell-null *Spib*-deficient mice show high susceptibility to *Citrobacter rodentium*-induced infectious colitis.[61] Moreover, mice lacking PPs show no gastritis with *Helicobacter pylori* infection. The coccoid but not helical form of *H. pylori* is captured by DCs residing in the SED, and CD4⁺ T cells are likely primed with antigens in PPs.[62] Collectively, these data indicate the importance of PPs for inducing immune responses against gastric and colonic infections. Furthermore, the deficiency of GP2 leads to reduced systemic antigen-specific IgG responses.[4] In mice devoid of M cells caused by an epithelium-specific deficiency of NIK, serum IgA and IL-17A are poorly produced in dextran sulfate sodium-induced colitis and polymicrobial sepsis,[63] suggesting that PPs are also important for systemic immune responses. Future studies are needed to determine how GPR31-mediated LysoDC immune responses might contribute to intestinal and systemic immunity.

Lactic and pyruvic acids provide various health benefits to the host.[64,65] Lactic acid is produced by a number of commensals including *Lactobacillus*, whereas pyruvic acid is directly or indirectly generated by limited species, including *Lactobacillus*, *Lachnospiraceae bacterium*, and *Bifidobacterium* .[32,64,66] In human, symbiotics containing *Bifidobacterium lactis* and fructooligosaccharides lead to increased pyruvate in stool samples.[67] Given that GPR31 responds to pyruvic acid with a higher affinity than to lactic acid (half maximal effective concentration of mouse GPR31 for pyruvic and lactic acids: 110 nM and 400 μM, respectively),[32] the identification of commensal species that produce pyruvate in the small intestine is potentially important. Furthermore, the pyruvate and lactate – GPR31 axis may serve as a beneficial target for enhancing mucosal immunity by oral vaccination. In the human small intestine, GPR31 is selectively

expressed in cDC1s, and the stimulation of human cDC1s with GPR31 ligands induces dendrite elongation.[68] GPR31-expressing cells in human PPs should therefore be identified in the future for potential clinical applications.

Author contributions

CRediT: **Katsuhiro Nakanishi:** Formal analysis, Investigation, Writing – original draft; **Takayuki Ajiro:** Formal analysis, Investigation; **Kaito Yukishima:** Formal analysis, Investigation; **Yuki Tsukamoto:** Investigation; **Junichi Kikuta:** Investigation, Methodology; **Shinichiro Sawa:** Investigation, Methodology, Writing – review & editing; **Michio Tomura:** Methodology, Writing – review & editing; **Nozomi Kinoshita:** Investigation; **Wataru Shimanuki:** Formal analysis, Investigation; **Akio Suzuki:** Investigation, Methodology; **Shun Arai:** Investigation; **Kazuki Maeshima:** Investigation; **Takumi Ichisawa:** Investigation; **Tomoya Katakai:** Methodology, Writing – review & editing; **Haruko Hayasaka:** Methodology, Writing – review & editing; **Masaru Ishii:** Methodology; **Eiji Umemoto:** Conceptualization, Funding acquisition, Investigation, Project administration, Writing – original draft.

Disclosure statement

No potential conflict of interest was reported by the author(s).

ORCID

Eiji Umemoto ⓘD http://orcid.org/0000-0002-8255-7149

Data availability statement

Bulk RNA-seq data have been deposited at GEO (accession number: GSE295342) and are publicly available as of the date of publication.

References

1. Kiyono H, Fukuyama S. NALT- versus Peyer's-patch-mediated mucosal immunity. Nat Rev Immunol. 2004;4 (9):699–710. doi: 10.1038/nri1439.
2. Nakamura Y, Kimura S, Hase K. M cell-dependent antigen uptake on follicle-associated epithelium for mucosal immune surveillance. Inflammation Regener. 2018;38(1):15. doi: 10.1186/s41232-018-0072-y.
3. Dillon A, Lo DD. M cells: intelligent engineering of mucosal immune surveillance. Front Immunol. 2019;10:10. doi: 10.3389/fimmu.2019.01499.
4. Hase K, Kawano K, Nochi T, Pontes GS, Fukuda S, Ebisawa M, Kadokura K, Tobe T, Fujimura Y, Kawano S, et al. Uptake through glycoprotein 2 of FimH+ bacteria by M cells initiates mucosal immune response. Nature. 2009;462(7270):226–230. doi: 10.1038/nature08529.
5. Sansonetti PJ, Arondel J, Cantey JR, Prévost MC, Huerre M. Infection of rabbit Peyer's patches by Shigella flexneri: effect of adhesive or invasive bacterial phenotypes on follicle-associated epithelium. Infect Immun. 1996;64(7):2752–2764. doi: 10.1128/iai.64.7.2752-2764.1996.

6. Nakato G, Hase K, Suzuki M, Kimura M, Ato M, Hanazato M, Tobiume M, Horiuchi M, Atarashi R, Nishida N, et al. Cutting edge: Brucella abortus exploits a cellular prion protein on intestinal M cells as an invasive receptor. J Immunol. 2012;189(4):1540–1544. doi: 10.4049/jimmunol.1103332.

7. Autenrieth IB, Firsching R. Penetration of M cells and destruction of Peyer's patches by Yersinia enterocolitica: an ultrastructural and histological study. Journal Medical Microbiology. 1996;44(4):285–294. doi: 10.1099/00222615-44-4-285.

8. Jensen VB, Harty JT, Jones BD. Interactions of the invasive pathogens salmonella typhimurium, listeria monocytogenes, and Shigella flexneri with M cells and murine Peyer's patches. Infect Immun. 1998;66 (8):3758–3766. doi: 10.1128/IAI.66.8.3758-3766.1998.

9. Nikitas G, Deschamps C, Disson O, Niault T, Cossart P, Lecuit M. Transcytosis of listeria monocytogenes across the intestinal barrier upon specific targeting of goblet cell accessible E-cadherin. J Exp Med. 2011;208 (11):2263–2277. doi: 10.1084/jem.20110560.

10. Lecuit M, Dramsi S, Gottardi C, Fedor-Chaiken M, Gumbiner B, Cossart P. A single amino acid in E-cadherin responsible for host specificity towards the human pathogen listeria monocytogenes. EMBO J. 1999;18 (14):3956–3963. doi: 10.1093/emboj/18.14.3956.

11. Lecuit M, Vandormael-Pournin S, Lefort J, Huerre M, Gounon P, Dupuy C, Babinet C, Cossart P. A transgenic model for listeriosis: role of internalin in crossing the intestinal barrier. Science. 2001;292(5522):1722–1725. doi: 10.1126/science.1059852.

12. Chiba S, Nagai T, Hayashi T, Baba Y, Nagai S, Koyasu S. Listerial invasion protein internalin B promotes entry into ileal Peyer's patches in vivo. Microbiology Immunology. 2011;55(2):123–129. doi: 10.1111/j.1348-0421. 2010.00292.x.

13. Gessain G, Tsai YH, Travier L, Bonazzi M, Grayo S, Cossart P, Charlier C, Disson O, Lecuit M. PI3-kinase activation is critical for host barrier permissiveness to listeria monocytogenes. J Exp Med. 2015;212(2):165–183. doi: 10.1084/jem.20141406.

14. Mabbott NA, Donaldson DS, Ohno H, Williams IR, Mahajan A. Microfold (M) cells: important immunosurveillance posts in the intestinal epithelium. Mucosal Immunol. 2013;6(4):666–677. doi: 10.1038/mi.2013.30.

15. Neutra MR, Frey A, Kraehenbuhl J-P. Epithelial M cells: gateways for mucosal infection and immunization. Cell. 1996;86(3):345–348. doi: 10.1016/S0092-8674(00)80106-3.

16. Da Silva C, Wagner C, Bonnardel J, Gorvel JP, Lelouard H. The Peyer's patch mononuclear phagocyte System at steady state and during infection. Front Immunol. 2017;8:1254. doi: 10.3389/fimmu.2017.01254.

17. Luciani C, Hager FT, Cerovic V, Lelouard H. Dendritic cell functions in the inductive and effector sites of intestinal immunity. Mucosal Immunol. 2022;15(1):40–50. doi: 10.1038/s41385-021-00448-w.

18. Wagner C, Bonnardel J, Da Silva C, Spinelli L, Portilla CA, Tomas J, Lagier M, Chasson L, Masse M, Dalod M, et al. Differentiation paths of Peyer's patch LysoDCs are linked to sampling site positioning, migration, and T cell priming. Cell Rep. 2020;31(1):107479. doi: 10.1016/j.celrep.2020.03.043.

19. Wang J, Gusti V, Saraswati A, Lo DD. Convergent and divergent development among M cell lineages in mouse mucosal epithelium. J Immunol. 2011;187(10):5277–5285. doi: 10.4049/jimmunol.1102077.

20. Bonnardel J, Da Silva C, Henri S, Tamoutounour S, Chasson L, Montañana-Sanchis F, Gorvel J-P, Lelouard H. Innate and adaptive immune functions of peyer's patch monocyte-derived cells. Cell Rep. 2015;11(5):770–784. doi: 10.1016/j.celrep.2015.03.067.

21. Lelouard H, Henri S, De Bovis B, Mugnier B, Chollat-Namy A, Malissen B, et al. Pathogenic bacteria and dead cells are internalized by a unique subset of Peyer's patch dendritic cells that express lysozyme. Gastroenterology. 2010;138:173–84.e1–3. doi: 10.1053/j.gastro.2009.09.051.

22. Martínez-López M, Iborra S, Conde-Garrosa R, Mastrangelo A, Danne C, Mann ER, Reid DM, Gaboriau-Routhiau V, Chaparro M, Lorenzo MP, et al. Microbiota sensing by Mincle-Syk axis in dendritic cells regulates Interleukin-17 and -22 production and promotes intestinal barrier integrity. Immunity. 2019;50(2):446–61.e9. doi: 10.1016/j.immuni.2018.12.020.

23. Kim SH, Cho BH, Kim KS, Jang YS. Complement C5a promotes antigen cross-presentation by Peyer's patch monocyte-derived dendritic cells and drives a protective CD8+ T cell response. Cell Rep. 2021;35(2):108995. doi: 10.1016/j.celrep.2021.108995.

24. Hase K, Murakami T, Takatsu H, Shimaoka T, Iimura M, Hamura K, Kawano K, Ohshima S, Chihara R, Itoh K, et al. The membrane-bound chemokine CXCL16 expressed on follicle-associated epithelium and M cells mediates lympho-epithelial interaction in GALT. J Immunol. 2006;176(1):43–51. doi: 10.4049/jimmunol.176.1.43.

25. Iwasaki A, Kelsall BL. Localization of distinct Peyer's patch dendritic cell subsets and their recruitment by chemokines macrophage inflammatory protein (MIP)-3alpha, MIP-3beta, and secondary lymphoid organ chemokine. J Exp Med. 2000;191(8):1381–1394. doi: 10.1084/jem.191.8.1381.

26. Salazar-Gonzalez RM, Niess JH, Zammit DJ, Ravindran R, Srinivasan A, Maxwell JR, et al. CCR6-mediated dendritic cell activation of pathogen-specific T cells in Peyer's patches. Immunity. 2006;24:623–632. doi: 10. 1016/j.immuni.2006.02.015.

27. Kanaya T, Hase K, Takahashi D, Fukuda S, Hoshino K, Sasaki I, Hemmi H, Knoop KA, Kumar N, Sato M, et al. The ets transcription factor spi-B is essential for the differentiation of intestinal microfold cells. Nat Immunol. 2012;13(8):729–736. doi: 10.1038/ni.2352.

28. Zhao X, Sato A, Dela Cruz CS, Linehan M, Luegering A, Kucharzik T, Shirakawa A-K, Marquez G, Farber JM, Williams I, et al. CCL9 is secreted by the follicle-associated epithelium and recruits dome region Peyer's patch CD11b+ dendritic cells. J Immunol. 2003;171(6):2797–2803. doi: 10.4049/jimmunol.171.6.2797.

29. Niess JH, Brand S, Gu X, Landsman L, Jung S, McCormick BA, Vyas JM, Boes M, Ploegh HL, Fox JG, et al. CX3CR1-mediated dendritic cell access to the intestinal lumen and bacterial clearance. Science. 2005;307 (5707):254–258. doi: 10.1126/science.1102901.

30. Bogunovic M, Ginhoux F, Helft J, Shang L, Hashimoto D, Greter M, Liu K, Jakubzick C, Ingersoll MA, Leboeuf M, et al. Origin of the lamina propria dendritic cell network. Immunity. 2009;31(3):513–525. doi: 10.1016/j.immuni.2009.08.010.

31. Mazzini E, Massimiliano L, Penna G, Rescigno M. Oral tolerance can be established via gap junction transfer of fed antigens from CX3CR1+ macrophages to CD103+ dendritic cells. Immunity. 2014;40(2):248–261. doi: 10.1016/j.immuni.2013.12.012.

32. Morita N, Umemoto E, Fujita S, Hayashi A, Kikuta J, Kimura I, Haneda T, Imai T, Inoue A, Mimuro H, et al. GPR31-dependent dendrite protrusion of intestinal CX3CR1+ cells by bacterial metabolites. Nature. 2019;566 (7742):110–114. doi: 10.1038/s41586-019-0884-1.

33. Liu Q, Umemoto E, Morita N, Kayama H, Baba Y, Kurosaki T, Okumura R, Takeda K. Pyruvate enhances oral tolerance via GPR31. Int Immunol. 2022;34(7):343–352. doi: 10.1093/intimm/dxac010.

34. Tomura M, Hata A, Matsuoka S, Shand FH, Nakanishi Y, Ikebuchi R, Ueha S, Tsutsui H, Inaba K, Matsushima K, et al. Tracking and quantification of dendritic cell migration and antigen trafficking between the skin and lymph nodes. Sci Rep. 2014;4(1):6030. doi: 10.1038/srep06030.

35. Jung S, Aliberti J, Graemmel P, Sunshine MJ, Kreutzberg GW, Sher A, Littman DR. Analysis of fractalkine receptor CX(3)CR1 function by targeted deletion and green fluorescent protein reporter gene insertion. Mol Cell Biol. 2000;20(11):4106–4114. doi: 10.1128/MCB.20.11.4106-4114.2000.

36. Uematsu S, Fujimoto K, Jang MH, Yang BG, Jung YJ, Nishiyama M, Sato S, Tsujimura T, Yamamoto M, Yokota Y, et al. Regulation of humoral and cellular gut immunity by lamina propria dendritic cells expressing Toll-like receptor 5. Nat Immunol. 2008;9(7):769–776. doi: 10.1038/ni.1622.

37. Manjunath N, Shankar P, Wan J, Weninger W, Crowley MA, Hieshima K, Springer TA, Fan X, Shen H, Lieberman J, et al. Effector differentiation is not prerequisite for generation of memory cytotoxic T lymphocytes. J Clin Invest. 2001;108(6):871–878. doi: 10.1172/JCI13296.

38. Hama H, Hioki H, Namiki K, Hoshida T, Kurokawa H, Ishidate F, Kaneko T, Akagi T, Saito T, Saido T, et al. ScaleS: an optical clearing palette for biological imaging. Nat Neurosci. 2015;18(10):1518–1529. doi: 10.1038/nn.4107.

39. Becattini S, Littmann ER, Carter RA, Kim SG, Morjaria SM, Ling L, Gyaltshen Y, Fontana E, Taur Y, Leiner IM, et al. Commensal microbes provide first line defense against listeria monocytogenes infection. J Exp Med. 2017;214(7):1973–1989. doi: 10.1084/jem.20170495.

40. Busch DH, Vijh S, Pamer EG. Animal model for infection with listeria monocytogenes. In: Current protocols in immunology. 2001. Chapter 19:Unit 19.9. John Wiley & Sons, Inc. doi: 10.1002/0471142735.im1909s36.

41. Lelouard H, Fallet M, de Bovis B, Méresse S, Gorvel JP. Peyer's patch dendritic cells sample antigens by extending dendrites through M cell-specific transcellular pores. Gastroenterology. 2012;142:592–601.e3. doi: 10.1053/j.gastro.2011.11.039.

42. Chai Q, Onder L, Scandella E, Gil-Cruz C, Perez-Shibayama C, Cupovic J, Danuser R, Sparwasser T, Luther S, Thiel V, et al. Maturation of lymph node fibroblastic reticular cells from myofibroblastic precursors is critical for antiviral immunity. Immunity. 2013;38(5):1013–1024. doi: 10.1016/j.immuni.2013.03.012.

43. Schmidt TH, Bannard O, Gray EE, Cyster JG. CXCR4 promotes B cell egress from Peyer's patches. J Exp Med. 2013;210(6):1099–1107. doi: 10.1084/jem.20122574.

44. Skoberne M, Schenk S, Hof H, Geginat G. Cross-presentation of listeria monocytogenes-derived CD4 T cell epitopes. The J Immunol. 2002;169(3):1410–1418. doi: 10.4049/jimmunol.169.3.1410.

45. Gul A, Pewe LL, Willems P, Mayer R, Thery F, Asselman C, Aernout I, Verbeke R, Eggermont D, Van Moortel L, et al. Immunopeptidomics mapping of listeria monocytogenes T cell epitopes in mice. Mol & Cellular Proteomics. 2024;23(9):100829. doi: 10.1016/j.mcpro.2024.100829.

46. Cheers C, McKenzie IF. Resistance and susceptibility of mice to bacterial infection: genetics of listeriosis. Infect Immun. 1978;19(3):755–762. doi: 10.1128/iai.19.3.755-762.1978.

47. Rescigno M, Urbano M, Valzasina B, Francolini M, Rotta G, Bonasio R, Granucci F, Kraehenbuhl J-P, Ricciardi-Castagnoli P. Dendritic cells express tight junction proteins and penetrate gut epithelial monolayers to sample bacteria. Nat Immunol. 2001;2(4):361–367. doi: 10.1038/86373.

48. Rescigno M, Rotta G, Valzasina B, Ricciardi-Castagnoli P. Dendritic cells shuttle microbes across gut epithelial monolayers. Immunobiology. 2001;204(5):572–581. doi: 10.1078/0171-2985-00094.

49. Hase K, Ohshima S, Kawano K, Hashimoto N, Matsumoto K, Saito H. Distinct gene expression profiles characterize cellular phenotypes of follicle-associated epithelium and M cells. DNA Res. 2005;12(2):127–137. doi: 10.1093/dnares/12.2.127.

50. Jinnohara T, Kanaya T, Hase K, Sakakibara S, Kato T, Tachibana N, Sasaki T, Hashimoto Y, Sato T, Watarai H, et al. IL-22BP dictates characteristics of Peyer's patch follicle-associated epithelium for antigen uptake. J Exp Med. 2017;214(6):1607–1618. doi: 10.1084/jem.20160770.

51. Kanaya T, Jinnohara T, Sakakibara S, Tachibana N, Sasaki T, Kato T, Riemann M, Jin J, Shiroguchi K, Kawakami E, et al. RelB and C/EBPα critically regulate the development of Peyer's patch mononuclear phagocytes. Mucosal Immunol. 2025;18(1):151–161. doi: 10.1016/j.mucimm.2024.10.005.

52. Chabot S, Wagner JS, Farrant S, Neutra MR. Tlrs regulate the gatekeeping functions of the intestinal follicle-associated epithelium. J Immunol. 2006;176(7):4275–4283. doi: 10.4049/jimmunol.176.7.4275.

53. Chieppa M, Rescigno M, Huang AY, Germain RN. Dynamic imaging of dendritic cell extension into the small bowel lumen in response to epithelial cell TLR engagement. J Exp Med. 2006;203(13):2841–2852. doi: 10.1084/jem.20061884.

54. Inamoto T, Furuta K, Han C, Uneme M, Kano T, Ishikawa K, Kaito C. Short-chain fatty acids stimulate dendrite elongation in dendritic cells by inhibiting histone deacetylase. The FEBS J. 2023;290(24):5794–5810. doi: 10.1111/febs.16945.

55. Kolesnikov M, Curato C, Zupancic E, Florindo H, Shakhar G, Jung S. Intravital visualization of interactions of murine Peyer's patch-resident dendritic cells with M cells. Eur J Immunol. 2020;50(4):537–547. doi: 10.1002/eji.201948332.

56. Rochereau N, Drocourt D, Perouzel E, Pavot V, Redelinghuys P, Brown GD, Tiraby G, Roblin X, Verrier B, Genin C, et al. Dectin-1 is essential for reverse transcytosis of glycosylated SIgA-antigen complexes by intestinal M cells. PLOS Biol. 2013;11(9):e1001658. doi: 10.1371/journal.pbio.1001658.

57. Sakhon OS, Ross B, Gusti V, Pham AJ, Vu K, Lo DD. M cell-derived vesicles suggest a unique pathway for trans-epithelial antigen delivery. Tissue Barriers. 2015;3(1–2):e1004975. doi: 10.1080/21688370.2015.1004975.

58. Hsieh CS, Macatonia SE, Tripp CS, Wolf SF, O'Garra A, Murphy KM. Development of TH1 CD4+ T cells through IL-12 produced by Listeria-induced macrophages. Science. 1993;260(5107):547–549. doi: 10.1126/science.8097338.

59. Disson O, Blériot C, Jacob JM, Serafini N, Dulauroy S, Jouvion G, Fevre C, Gessain G, Thouvenot P, Eberl G, et al. Peyer's patch myeloid cells infection by listeria signals through gp38+ stromal cells and locks intestinal villus invasion. J Exp Med. 2018;215(11):2936–2954. doi: 10.1084/jem.20181210.

60. Kishikawa S, Sato S, Kaneto S, Uchino S, Kohsaka S, Nakamura S, Kiyono H. Allograft inflammatory factor 1 is a regulator of transcytosis in M cells. Nat Commun. 2017;8(1):14509. doi: 10.1038/ncomms14509.

61. Nakamura Y, Mimuro H, Kunisawa J, Furusawa Y, Takahashi D, Fujimura Y, Kaisho T, Kiyono H, Hase K. Microfold cell-dependent antigen transport alleviates infectious colitis by inducing antigen-specific cellular immunity. Mucosal Immunol. 2020;13(4):679–690. doi: 10.1038/s41385-020-0263-0.

62. Nagai S, Mimuro H, Yamada T, Baba Y, Moro K, Nochi T, Kiyono, H, Suzuki, T, Sasakawa, C, Koyasu, S. Role of Peyer's patches in the induction of helicobacter pylori-induced gastritis. Proceedings of the National Academy of Sciences of the United States of America; Vol. 104. 2007. p. 8971–8976. doi: 10.1073/pnas.0609014104.

63. Ramakrishnan SK, Zhang H, Ma X, Jung I, Schwartz AJ, Triner D, Devenport SN, Das NK, Xue X, Zeng MY, et al. Intestinal non-canonical NFκB signaling shapes the local and systemic immune response. Nat Commun. 2019;10(1):660. doi: 10.1038/s41467-019-08581-8.

64. Deng S, Cao H, Li T, Wang X, Meng J, Zeng T, Zhang D, Zhang S, Wang G, Liu R, et al. Lachnospiraceae-bacterium alleviates ischemia-reperfusion injury in steatotic donor liver by inhibiting ferroptosis via the Foxo3-Alox15 signaling pathway. Gut Microbes. 2025;17(1):2460543. doi: 10.1080/19490976.2025.2460543.

65. Sauer M, Han NS, Mattanovich D, Ivan Nikel P. Lactic acid bacteria: little helpers for many human tasks. Essays In Biochem. 2021;65(2):163–171. doi: 10.1042/EBC20200133.

66. Zhang B, Qiu J, Qu Z, Xiao R, Wang L, Tian P, Zhang H, Chen W, Wang G. Bifidobacterium adolescentis FJSSZ23M10 modulates gut microbiota and metabolism to alleviate obesity through strain-specific genomic features. Food Funct. 2025;16(6):2415–2431. doi: 10.1039/D4FO06449F.

67. Crovesy L, El-Bacha T, Rosado EL. Modulation of the gut microbiota by probiotics and symbiotics is associated with changes in serum metabolite profile related to a decrease in inflammation and overall benefits to metabolic health: a double-blind randomized controlled clinical trial in women with obesity. Food Funct. 2021;12(5):2161–2170. doi: 10.1039/d0fo02748k.

68. Oguro-Igashira E, Murakami M, Mori R, Kuwahara R, Kihara T, Kohara M, Fujiwara M, Motooka D, Okuzaki D, Arase M, et al. The pyruvate–GPR31 axis promotes transepithelial dendrite formation in human intestinal dendritic cells. Proc Natl Acad Sci USA. 2024;121(44):e2318767121. doi: 10.1073/pnas.2318767121.